ML-TOMCAT: Machine-Learning-Based Satellite-Corrected Global Stratospheric Ozone Profile ~~Dataset~~ Data Set from a Chemical Transport Model

Sandip S. Dhomse[1,2], Carlo Arosio[3], Wuhu Feng[1,4], Alexei Rozanov[3], Mark Weber[3], and Martyn P. Chipperfield[1,2]

[1]School of Earth and Environment, University of Leeds, Leeds, UK
[2]National Centre for Earth Observation, University of Leeds, Leeds, UK
[3]Institute for Environmental Physics, University of Bremen, Bremen, Germany
[4]National Centre for Atmospheric Science, University of Leeds, Leeds, UK

Correspondence: Sandip S. Dhomse (s.s.dhomse@leeds.ac.uk)

Abstract.

High quality stratospheric ozone profile ~~datasets~~ data sets are a key requirement for accurate quantification and attribution of long-term ozone changes. Satellite instruments ~~obtain~~ provide stratospheric ozone profile measurements over typical mission durations of 5-15 years. Various methodologies have then been applied to merge and homogenise the different satellite data in order to create longer term observation-based ozone profile ~~datasets~~ data sets with minimal data gaps. However, individual satellite instruments use different measurement methods, sampling patterns and retrieval algorithms which complicate the merging of these different ~~datasets~~data sets. In contrast, atmospheric chemical models can produce chemically consistent long-term ozone simulations based on specified changes in external forcings, but they are subject to the deficiencies associated with incomplete understanding of complex atmospheric processes and uncertain photochemical parameters.

Here, we use chemically self-consistent output from the TOMCAT 3-D chemical transport model (CTM) and a Random-Forest (RF) ensemble learning method to create a merged 42-year (1979-2020) stratospheric ozone profile ~~dataset~~ data set (ML-TOMCAT V1.0). The underlying CTM simulation was forced by meteorological reanalyses, specified trends in long-lived source ~~gas~~gases, solar flux and aerosol variations. The RF is trained using the Stratospheric Water and OzOne Satellite Homogenized (SWOOSH) ~~dataset~~ data set over the time periods of the Microwave Limb Sounder (MLS) from the Upper Atmosphere Research Satellite (UARS) (1991-1998) and Aura (2005-2016) missions. We find that ML-TOMCAT shows excellent agreement with available independent satellite-based ~~datasets~~ data sets which use pressure as ~~the~~ vertical coordinate (e.g. GOZCARDS, SWOOSH for non-MLS periods) but weaker agreement with the ~~datasets which are height-based~~ data sets which are altitude-based (e.g. SAGE–CCI–OMPS, SCIAMACHY-OMPS). We find that at almost all stratospheric levels ML-TOMCAT ozone concentrations are well within uncertainties ~~in the observational datasets~~of the observational data sets. The ML-TOMCAT ~~dataset is thus~~ (V1.0) data set is ideally suited for the evaluation of chemical model ozone profiles from the tropopause to 0.1 hPa ~~. ML-TOMCAT data~~ and is freely available via https://zenodo.org/record/4997959#.YNzleUlKiUk (Dhomse et al., 2021) .

1 Introduction

With the successful implementation of the Montreal Protocol, various observations confirm reductions in the concentrations of ~~ozone depleting~~ halogenated ozone-depleting substances (ODSs) in the atmosphere (WMO, 2014, 2018). Satellite data records also confirm a peak in upper stratospheric HCl (the main chlorine reservoir) around 1997, followed by a steady decline (Anderson et al., 2000; Froidevaux et al., 2006a; Hossaini et al., 2019). Hence, attention has turned towards the detection and attribution of ozone recovery ~~(e.g. Dhomse et al., 2006; Solomon et al., 2016; Chipperfield et al., 2017; Dhomse et al., 2018)~~ (e.g. Dhomse et al., However, the accurate quantification of ozone changes is challenging because of the quality of long-term ozone profile ~~datasets~~data sets, where measurement errors are of similar ~~magnitude or larger~~ or larger magnitude than the long-term ozone trends. In addition, complex coupling between various physical and chemical processes controlling stratospheric ozone concentrations cause large short-term ozone changes. Complications also arise because there are some non-linear changes in stratospheric dynamics as well as chemical constituents. For example, between 2018 and 2021, some of the largest and smallest ozone losses of the recent decades were recorded in both the Arctic and Antarctic polar stratospheres (e.g. Wargan et al., 2020; Wohltmann et al., 2020; Bognar et al., 2021; Weber et al., 2021). Some observational data suggest that there has been a continuous decline in lower stratospheric ozone (Ball et al., 2018, 2020), which could be attributed to changes in stratospheric dynamics (e.g. Chipperfield et al., 2018; Wargan et al., 2018; Orbe et al., 2020; Abalos and de la Cámara, 2020). Atmospheric concentrations of ODSs such as CFC-11 are decreasing at uneven rates (Montzka et al., 2018, 2021) which could induce variability in ozone trends. Additionally, significant positive trends have been detected in very short-lived substances (VSLS) containing chlorine and bromine that are not controlled by the Montreal Protocol (e.g. Hossaini et al., 2015, 2019).

As there ~~is~~ are no long-term ozone profile data from a single satellite instrument, various attempts have been made to merge such data from different instruments. However, individual satellite instruments have different temporal and spatial resolution depending on the measurement techniques and retrieval algorithms ~~(e.g. Damadeo et al., 2018)~~ (e.g. Sofieva et al., 2014; Damadeo et al., 20 For example, solar occultation instruments (e.g. Stratospheric Aerosol and Gas Experiment (SAGE, McCormick et al., 1989), Halogen Occultation Experiment (HALOE, Russell III et al., 1993)) provide high quality measurements but are constrained by limited spatial coverage. Limb-scanning instruments such as the Microwave Limb Sounder (MLS, Froidevaux et al., 2006b), Scanning Imaging Absorption Spectrometer for Atmospheric Cartography (SCIAMACHY, Bovensmann et al., 1999), Optical Spectrograph and InfraRed Imager System (OSIRIS, Murtagh et al., 2002) provide better spatial coverage but have coarser vertical resolution. A key constraining factor is that only few satellite ~~datasets~~ data sets cover enough overlapping years to remove inter-instrument biases with minimal uncertainty.

Hence, Randel and Wu (2007) adopted a novel approach to create a gap-free stratospheric ozone profile data for the 1979–2005 time period. They used SAGE (I and II) satellite profile measurements and polar ozonesondes, together with a seasonally varying ozone climatology from Paul et al. (1998) to fill the gaps, to generate multi-variate ~~regression based~~ regression-based gap-free ozone anomalies. Later, Cionni et al. (2011) used a similar methodology along with climate model simulations to extend the time series backwards to 1850. The Cionni et al. (2011) data ~~was~~ were recommended for the historical CMIP5 simulations ~~, in order to enforce time-dependent ozone variations, for the~~ for the climate models that did not include stratospheric chemistry, in order to enforce time-dependent ozone variations. Hassler et al. (2008) used a different methodology to create a satellite-based long-term ozone profile ~~dataset~~data set. Along with SAGE I and II measurements, they used HALOE and POAM (Polar Ozone and Aerosol Measurement) II and III satellite measurements, as well as ozonesonde data from 130 stations, to create a collection of binary data files; also known as the "Binary DataBase of Profiles" (BDBP) version 1.0. Bodeker et al. (2013) ~~,~~ updated the BDBP ~~dataset~~ data set to construct “Bodeker Scientific” or “BS” data. They updated BDBP data by including measurements from the Limb Infrared Monitor of the Stratosphere (LIMS), the Improved Limb Array Spectrometer (ILAS), and ILAS II. They used a multivariate regression model to create different versions of the ozone profile ~~dataset~~ data set ranging from the surface to 70 km for the 1979-2008 time period. Hassler et al. (2018a) revised ~~the Bodeker et al. (2013) dataset~~ and extended (1979–2016) the "BS" data set by using the TOMCAT chemical transport model (CTM) ozone profiles as a transfer function to capture ozone variability for the period without satellite observations.

Another widely used merged data set is the Global OZone Chemistry And Related trace gas Data records for the Stratosphere (GOZCARDS, Froidevaux et al., 2015). These are monthly mean ~~zonal mean~~ zonally averaged time series constructed using ozone ~~profiles~~ profile measurements from several NASA satellite instruments and the Atmospheric Chemistry Experiment - Fourier Transform Spectrometer (ACE-FTS, Bernath et al., 2005). Merging is done primarily by removing average biases between SAGE II and individual data records for overlap periods (Froidevaux et al., 2015). The GOZCARDS data files contain mixing ratios on a pressure–latitude grid (300 hPa to 0.1 hPa), updated later to GOZCARDS v2.2 (Froidevaux et al., 2019).

Davis et al. (2016) adopted a slightly different approach to construct the Stratospheric Water and Ozone Satellite Homogenized (SWOOSH) data set. SWOOSH merges stratospheric ozone profile data from solar occultation instruments (SAGE-II/III, HALOE, ACE-FTS) as well as limb-scanning instruments (UARS-MLS, and Aura-MLS). The measurements are homogenized by applying corrections that are calculated from data taken during time periods of instrument overlap. The primary SWOOSH data product consists of monthly mean zonal-mean values on a pressure grid at 2.5, 5 and 10 degree resolution. One of the major characteristics of SWOOSH data is that when merging greater weight is given to the instruments that sample more frequently (e.g. Aura-MLS). Filled and unfilled versions of the ~~dataset~~ data set exist on both geographical and equivalent latitude coordinates.

Several ~~other~~ additional attempts have been made to merge satellite time series from limb and occultation instruments. ~~In this study we consider~~ For example, the SAGE–CCI–OMPS ~~dataset~~data set, described in Sofieva et al. (2017) ~~, which~~ includes SAGE II time series and several limb ~~datasets~~data sets. The OMPS-LP ~~dataset~~ data set used is produced at the University of Saskatoon (Zawada et al., 2018). ~~The CCI data sets were firstly~~ First, they screened and homogenized CCI data sets in the HARMOZ format ~~and then merged~~ before merging them in terms of ozone anomalies~~with the SAGE II and OMPS-LP observations.~~

~~Arosio et al. (2019) also~~ . Recently, Arosio et al. (2019) created a merged SCIAMACHY-OMPS limb ~~merged dataset~~ data set (SCIA-OMPS), which combines these two time series produced at the University of Bremen. They ~~use~~ used MLS data series as a transfer function to merge SCIAMACHY with OMPS-LP as these instruments share only two months of overlap, but MLS was not included in the merged ~~dataset~~data set. This time series is monthly averaged, covers the period 2002-present and is longitudinally resolved, with a ~~5°~~ 5° latitude × ~~20°~~ 20° longitude grid. Due to the similarities in the measurement geometries and techniques, and in the retrieval approaches, ~~a plain debiasing approach was implemented~~they implemented a plain de-biasing approach for the merging, directly obtaining a long-term ozone time series in appropriate units.

Another widely accepted approach is using data assimilation techniques to create observation-based data (e.g. Feng et al., 2008; Skachko However, only a few instruments such as MLS provide relatively long-term ozone profile measurements. For the pre-MLS time period, very few observations are available that can provide good constraint on the assimilation system. Also, the forward model is generally forced with available (re)analysis dynamical fields so reanalysis data sets are also prone to the inhomogenities in the forcing fields along with any discrepancies in chemical scheme.

In this paper we present a new data-model method for producing a long-term ~~dataset~~ data set of stratospheric ozone. We use ozone profile output from a CTM to create a machine-learning-based satellite-corrected long-term chemically (and dynamically) consistent ozone profile ~~dataset~~ data set (hereafter, ML-TOMCAT) for the ~~1979–2020~~ 1979 – 2020 time period. The CTM setup is described in Section 2, followed by our methodology in Section 3. Comparisons of ML-TOMCAT with some of the other available merged ozone profile ~~datasets~~ data sets are presented in Section 4, with a summary of our key results in Section 5.

2 Model Setup

We use chemically consistent monthly mean zonal mean ozone profiles from the TOMCAT ~~chemical transport model (CTM)~~ CTM as the basis ~~dataset~~data set. TOMCAT is an off-line three-dimensional (3D) CTM that includes a comprehensive stratospheric chemistry scheme (Chipperfield, 2006). For the present study, the CTM setup is similar to the control simulations used in our recent studies such as Feng et al. (2021); Bognar et al. (2021) and Weber et al. (2021). Briefly, ~~the model~~ TOMCAT is forced with meteorological fields from ERA-5 reanalyses (Hersbach et al., 2020), starting from 1979. Simulations are performed at a 2.8 $\times$ 2.8 degree horizontal resolution with 32 hybrid sigma-pressure levels extending from the surface to about 60 km. For major ODSs and GHGs the model uses time-dependent observed global mean surface mixing ratios (Carpenter et al., 2018) that are treated as well-mixed throughout the troposphere. The model also includes the effects of solar flux variability and heterogeneous chemistry on volcanically enhanced stratospheric aerosol as described in ~~Dhomse et al. (2015, 2016)~~ Dhomse et al. (2015, 2016) . Solar irradiance data are from the NRL2 (Coddington et al., 2016) empirical model and the ~~sulphate~~ sulfate aerosol surface area density (SAD) from Luo (2016). ~~The model~~ TOMCAT also includes chlorine and bromine contributions from VSLS as described in Hossaini et al. (2019). ~~The model~~ A passive ozone tracer (no chemical ozone loss), generally used to diagnose chemical ozone loss, is initialised every six months from the chemical ozone tracer (1st June and 1st December). TOMCAT has been regularly used to study long-term changes in stratospheric trace gases, showing good agreement with various ground-based and satellite ~~datasets (e.g. Mahieu et al., 2014; Chipperfield et al., 2015; Wales e~~ sets (e.g. Mahieu et al., 2014; Chipperfield et al., 2015; Wales et al., 2018; Harrison et al., 2021; Prignon et al., 2021) .

3 Methodology

We use the Random Forest (RF) regression analysis to generate a long-term chemically consistent ~~dataset~~data set. The RF is a supervised machine learning (ML) algorithm that uses an ensemble of decision trees (e.g. Breiman, 2001; Svetnik et al., 2003). ~~Decision treesuse a binary recursive classifying algorithm by splitting observations into two homologous groups. The recursive nature of the algorithm means splitting could be repeated until only two observations are left in the final split.~~A decision tree can be considered as a flow chart used in computer programming (a tree-shaped schematic) that is generally used to show a statistical probability or path of action. A single decision tree in a RF can be considered as a random tree in a forest of decision trees. Each decision tree consists of three components: decision nodes, leaf nodes, and a root node. The root node and decision nodes of the decision tree represent the explanatory variables. The leaf node represents the final output. The explanatory variables used in our analysis are explained at end of this section.

A decision tree algorithm divides the data set into branches (using true and false criterion), which further segregate into other branches until a leaf node (or result node) is reached. Multiple trees are constructed by randomly sampling data points multiple times (e.g. bootstrap method). Hence, an individual tree can be considered as unique tree (hence unique output). RF uses a bagging technique, that means the RF model consists of many individual ~~trees or learners~~ decision trees and aggregated predictions are used for the final prognosis. A distinct advantage of RF regression is that it ~~can~~ is relatively accurate and very easy to set up. RF can also behave like a non-linear regression method. As RF adds randomness to the ~~model~~decision procedure, instead of relying on the most important ~~feature~~explanatory variables, it searches for the best ~~feature~~ variable among random subsets. This ensures that the final output does not rely heavily on a single ~~learner~~explanatory variable, thereby avoiding ~~overfitting~~ over-fitting (e.g. Kotsiantis, 2013). We use ~~Random Forest (RF)~~ RF Regression from the Python package ~~sklearn~~ Sci-kit learn (Pedregosa et al., 2011) with two options: *random_state=0*, and *bootstrap=True*.

Initially, TOMCAT zonal mean ozone profiles are linearly interpolated in log-pressure space on to 43 equidistant (12 per decade) pressure levels (1000–0.1 hPa, MLS pressure levels), followed by spatial interpolation ~~on to~~ onto 72 SWOOSH latitude bins at 2.5° resolution. SWOOSH data ~~is~~ are obtained via https://csl.noaa.gov/groups/csl8/swoosh/. Then, we calculate the ozone difference (dO_3) between SWOOSH and model ozone profiles for the 1991-1998 and 2005-2016 time periods (total 20 years). For the calculation of dO_3 values, we use the gap-filled SWOOSH data product. SWOOSH data ranges from 316 to 1 hPa (31 pressure levels), hence dO_3 for pressure levels below 316 hPa are linearly ~~interpolated~~ extrapolated by approximating dO_3 at 1000 hPa to be about 0.01 ppm. Similarly, for levels above 1 hPa, we use linear interpolation assuming that dO_3 at 0.1 hPa is about -0.1 ppm, based on bias seen with respect to Aura MLS measurements (Livesey et al., 2020) .

For the regression analysis, a 20-year (largely MLS covering) time period is selected in order to avoid heteroscedasticity (i.e. effect of different sampling frequencies/methodologies (e.g. Sofieva et al., 2014; Millán et al., 2016) between different types of satellite ~~datasets~~data sets) as SWOOSH relies heavily on MLS (UARS and Aura) data records. Additionally, it also covers a period when the stratospheric chlorine loading was increasing (1991-1998) and decreasing (2005-2016) and RF has enough sample to include different characteristics of ozone variability. The regression model has 5 terms: Passive ozone (PO_3), HCl mixing ratio (HCl), methane mixing ratio (CH_4) as well as observation-model total column difference ($dTCO$) and Mg II solar flux term ($MgII$). The PO_3, HCl and CH_4 terms account for possible biases in CTM profiles due to transport in different stratospheric regions (e.g. Strahan et al., 2011; Feng et al., 2021). $dTCO$ is an ideal learner for the lower stratospheric ozone transport as total column ozone measurements have much smaller retrieval errors (e.g. Petropavlovskikh et al., 2019), hence they provide a good constraint for the possible biases in ERA-5 stratospheric transport (e.g. Ploeger et al., 2021). TOMCAT has 203 spectral bins in the photolysis scheme (e.g. Dhomse et al., 2016). Hence, the $MgII$ solar flux term is included to account for possible biases in the representation of the 11-year solar flux variability (e.g. Haigh et al., 2010; Dhomse et al., 2013) or the use of coarse spectral bins (e.g. Sukhodolov et al., 2016).

Overall, there are ~~thus five learners~~ five explanatory variables in the regression model ~~that~~ for individual grid points and these are taken from TOMCAT output fields. The regression model can be represented as:

$$dO_3 = \beta_1 PO_3 + \beta_2 HCl + \beta_3 CH_4 + \beta_4 dTCO + \beta_5 MgII + residuals \quad (1)$$

where β_1, β_2, β_3, β_4 and β_5 can be considered as the contribution coefficient for a given explanatory variable and PO_3, HCl, CH_4 are TOMCAT monthly mean zonal mean tracers. For the calculation of $dTCO$ we use Copernicus Climate Change Service (C3S) total ozone data (1979–2018). The C3S total column product is a combination of total column data from 15 sensors using gap-filling assimilation methods and is obtained via https://cds.climate.copernicus.eu/cdsapp#!/dataset/satellite-ozone?tab=overview (last access: 1 May 2021). For the years 2019 and 2020, we use level 3 total column data from the Ozone Monitoring instrument (OMI) V3 that is obtained via https://search.earthdata.nasa.gov (last access: 1 May 2021). The Mg II index is obtained from http://www.iup.uni-bremen.de/UVSAT/datasets/mgii (last access: 1 May 2021). We assume long-term chemical ozone changes are realistically represented by TOMCAT chemistry (e.g. Feng et al., 2007; Chipperfield et al., 2017; Dhomse et al., 2019)~~and so~~ , hence all the predictor time series are detrended and normalised between 0 to 1.

4 Results

Atmospheric chemical models are ideal tools for understanding/simulating past (and future) ozone changes, as they combine up-to-date knowledge about various physical and chemical processes using a mathematically consistent framework. Different models use different combinations of chemical and dynamical schemes to represent important processes in the atmosphere. However, some of these processes are computationally expensive, hence they are represented by somewhat simplified parameterisations. For example, many chemical models prescribe observation-based ~~sulphate~~ sulfate surface area density (SAD) to represent the effects of volcanically enhanced stratospheric aerosol ~~to simulate~~ for simulating heterogeneous chemistry which leads to ozone loss (Dhomse et al., 2015). Many models also prescribe surface concentrations of ~~GHGs~~ greenhouse gases (GHGs) and ODSs rather than emission fluxes. CTMs such as TOMCAT use dynamical forcing fields from (re)analyses ~~datasets~~ data sets such as ERA-Interim or ERA-5. Hence CTMs are subject to ~~the~~ possible inhomogeneities due to changes in the number of assimilated observations, as well as other deficiencies (e.g. missing processes) in the forward model used in the assimilation system. On the other hand, observational ~~datasets~~ data sets are also subject to errors associated with the measurement techniques, instrument degradation and retrieval algorithms. Hence, almost all chemical models may be expected to show a bias against observational data records, either because of model deficiencies or errors in the ~~observational datasets~~observations. However, chemical models do use a consistent chemical scheme, so we can assume that ~~model-observations~~ chemical model-observation ozone differences are largely due to uncertainties in the forcing fields such as meteorology (e.g. winds, temperature) and chemical parameterisations (e.g. reaction rates, solar fluxes, photolysis schemes). CTMs have the distinct advantage in terms of dynamics as they are forced with up-to-date reanalysis data, although with the above-noted caveat of possible inhomogeneities in observations used in the assimilation systems. ~~Therefore,~~ Hence, recently initiated SPARC Reanalysis Intercomparison project (S-RIP) is aimed at providing guidance on future reanalysis activity. S-RIP also plans to perform comprehensive evaluation and intercomparison of different reanalysis data products; for details see https://www.sparc-climate.org/sparc-report-no-10. Here, we train the ML algorithm on the model-observation differences for the period that has relatively good temporal sampling. Estimated parameters are then used to simulate differences for the entire (1979–2020) time period. In this section, we analyse model-observation biases associated with individual predictors and compare the ML-corrected data against a variety of observation-based ~~datasets~~data sets.

4.1 Model biases

Figure 1 shows climatological (2006–2020) monthly zonal mean differences between ~~SWOOSH and TOMCAT ozone profiles.~~ TOMCAT ~~ozone~~ and SWOOSH ozone profiles (TOMCAT minus SWOOSH). TOMCAT profiles show an almost ~~symmetrical structure with positive~~ symmetrically structured negative biases in the upper stratosphere and ~~negative~~ positive biases in the lower stratosphere. ~~The largest positive~~ The largest negative biases (up to 0.8 ppm) occur in the tropical upper stratosphere (around 3 hPa) and they remain ~~positive~~ negative throughout the year. The ozone lifetime at these altitudes is less than a day, hence the observed biases might be associated with deficiencies in the photochemical reactions in the model. At this altitude, ozone production is largely controlled by solar fluxes below 240 nm while longer wavelengths control ozone destruction (e.g. Haigh et al., 2010). Therefore, negative ozone biases in the upper stratosphere are most probably due to uncertainties in the solar irradiances and/or photolysis cross sections that control ozone production (e.g. Brasseur and Solomon, 2006). Furthermore, in this region of the atmosphere, ozone chemistry is ~~very temperature-dependent~~ mostly temperature dependent (e.g. Stolarski et al., 2010; Dhomse et al., 2013, 2016), hence the model ozone biases could be due to uncertainties in temperature-dependent reaction rates (e.g. Ghosh et al., 1997).

In the lower stratosphere the ozone lifetime ranges from months to years, hence positive biases in the ~~modelled~~ TOMCAT ozone could be due to a combination of both dynamics and chemistry. First, reduced overhead ozone could increase lower stratospheric ozone via the self-healing effect, i.e. increased ultra-violet radiation increases ozone production at lower altitudes (e.g. Haigh, 1994). Second, ozone is primarily produced in the tropical stratosphere, and its downward transport is controlled by the ~~QBO~~ quasi-biennial oscillation (QBO) (e.g. Tian et al., 2006), whereas transport towards mid-high latitudes is determined by the strength of the Brewer-Dobson (BD) circulation ~~(e.g. Holton et al., 1995; Weber et al., 2003, 2011; Dhomse et al., 2006)~~ (e.g. Holto increases its lifetime considerably. Hence, ozone biases in the lower stratosphere are likely due to the incomplete representation of various circulation pathways in TOMCAT either due to model resolution or missing representation of key physical process in the ERA-5 reanalysis scheme (e.g. Mitchell et al., 2020) which impacts the meteorology used in the CTM.

4.2 ~~Learner contributions~~Contribution from explanatory variables

As the exact causes of ~~model~~ TOMCAT ozone biases are still not well understood, we use the RF model to remove ~~these biases in TOMCAT~~them. The RF regression model coefficients are derived using 20 years (1991–1998, 2006–2018) for which SWOOSH data includes a large number of observational profiles especially from MLS on the UARS and Aura satellite platforms. The RF regression model uses ~~20-years~~ 20 years of monthly data with 80% and 20% of data points being used for training and testing, respectively. ~~Estimated~~ The estimated RF regression coefficients are then used to calculate model biases for the entire 42-year time period (1979–2020). RF-calculated ozone biases are then added to the TOMCAT time series to create the long-term gap-free ~~dataset~~data set, hereafter labelled ML-TOMCAT.

Figure 2 shows how much variance (or R^2) of the data the RF regression model is able to explain, along with regression coefficients for individual ~~learners~~explanatory variables. For example, R^2 ~~equal to~~ value of 0.8 indicates that the RF regression model is able to explain 80% of the biases in ~~modelled~~ TOMCAT ozone relative to SWOOSH data for the 20 years of the training period. R^2 also represents sum of the regression coefficients from individual explanatory variables. Overall, the RF regression model performance is consistently high ($R^2 > 0.8$) throughout the stratosphere, except for the mid-stratosphere which is a transition region where the TOMCAT ozone biases change from positive to negative. At high northern latitudes, mid-stratospheric R^2 values decrease to 0.6. However, since ~~TOMCAT-SWOOSH~~ TOMCAT – SWOOSH differences are much smaller here, a RF-based correction has a minimal impact on the quality of ML-TOMCAT ozone profiles.

Additionally, as expected, the RF regression coefficients are significant in different regions of the stratosphere for various ~~learners~~explanatory variables. The passive ozone tracer seems to show the largest coefficients in the tropical mid-stratosphere, as well as varying contributions in different regions of the stratosphere. The passive ozone contribution in the tropical mid-stratospheric could be linked to the incomplete representation of NO_x-related chemical changes in TOMCAT and/or seasonal changes in the stratospheric transport in the re-analysis (e.g. Galytska et al., 2019). The HCl tracer shows significant coefficients in the upper stratosphere, where the ClO ozone loss cycle is important. It also shows significant contribution at low-mid-latitude lower stratosphere. HCl can be considered as both a dynamical and chemical proxy, as ~~well as~~ in the ~~tropical lower stratosphere.~~ upper stratospheric HCl is primarily produced via degradation of ozone-depleting substances and is transported downwards at high latitudes via the BD circulation (e.g. Mahieu et al., 2014) . Therefore, HCl variations in this region can be considered as a proxy for the changes in the strength of the BD circulation as well as horizontal isentropic transport, especially between tropics and mid-latitudes. The CH_4 tracer term seems to show significant coefficients in the lowermost stratosphere (just above the tropopause) as well as a significant contribution around the mid-latitude sub-tropics. The CH_4 tracer contribution resembles a QBO-induced secondary circulation pattern. Interestingly, the solar term shows the largest coefficients in the mid-latitude upper stratosphere rather than in the tropical upper stratosphere, suggesting solar flux variability has only a minor contribution to the ~~model-observation~~ TOMCAT-observation biases. As expected the $dTCO$ term shows the largest contribution in the lowermost stratosphere, especially in the tropical and polar regions. Interestingly, ozone anomalies in these regions show good agreement with various satellite-based data sets (e.g. Chipperfield et al., 2017, 2018; Li et al., 2020; Feng et al., 2021), and ~~model~~ TOMCAT biases are much smaller. This means that although $dTCO$ coefficients are largest in the lowermost stratosphere, the overall bias correction contribution remains relatively small.

4.3 Comparison against merged ~~datasets~~data sets

After analysing the regression coefficients, we now present a comparison between ML-TOMCAT and available satellite-based long-term ~~datasets.~~ data sets. Due to key differences between satellite measurement techniques, ozone profiles are retrieved either at ~~height~~ altitude or pressure levels and either in units of mixing ratio or number density. For example, MLS retrieves profiles of ozone mixing ratio on pressure levels whereas SAGE retrieves profiles of number density on ~~height~~ altitude levels. Hence, merging these different ~~datasets~~ data sets needs pressure, temperature or ~~height~~ altitude information at a given co-location from an external source such as reanalysis data. The GOZCARDS and SWOOSH ~~datasets~~ data sets use MERRA2 reanalysis data to convert SAGE II ozone number density profiles on fixed pressure levels (Damadeo et al., 2013). ~~Since,~~ ML-TOMCAT is based on modelled ozone profiles as a function of pressure, ~~conversion to height~~ although conversion to altitude (geopotential height) coordinates is straightforward. In particular, ML-TOMCAT data ~~was~~ were processed on corresponding grids/units using ERA-5 geopotential height, temperature and pressure fields that are used to drive TOMCAT.

This subsection consists of two parts. First we compare ML-TOMCAT profiles with ~~datasets~~ data sets using pressure coordinate systems (e.g. SWOOSH, GOZCARDS), followed by comparisons with ~~height-based datasets~~ altitude-based data sets (SAGE–CCI–OMPS, SCIA-OMPS, BSVert).

4.3.1 Comparison with pressure level data

As noted earlier, we used only 20 years of SWOOSH data to train the RF model. Hence, the next obvious step is to compare ML-TOMCAT ozone with SWOOSH over the full time period. Figure 3 compares relative differences (in ~~percentage~~percent) of ML-TOMCAT with GOZCARDS and SWOOSH, respectively, as a function of latitude and pressure. ML-TOMCAT shows slightly positive biases in the middle stratosphere and somewhat negative biases in the upper and lower stratosphere with respect to both SWOOSH and GOZCARDS data. The largest biases (up to 10%) are observed in the tropical lowermost stratosphere as well as polar latitudes. However, these largest differences in the tropical lowermost stratosphere (and upper troposphere) cannot be correctly validated as most satellite retrievals show largest their uncertainties in this region ~~(Rahpoe et al., 2015; Steinbrecht et al., 2017)~~ (Rahp
Similarly, ~~the~~ for the non-MLS period, the biases in the polar stratosphere could be due to the lack of observational ozone profiles during polar ~~nights~~night.

Figure 4 shows TOMCAT, ML-TOMCAT, SWOOSH and GOZCARDS ozone time series over the equator (0° lat) at 3 pressure levels (1, 10 and 50 hPa). Supplementary Figures S1 to S10 show similar comparisons at 15°N, 15°S, 30°N, 30°S, 45°N, 45°S, 60°N, 60°S, 75°N, and 75°S latitude bins. The grey shaded area indicates the standard deviation of the ozone values within each bin for the GOZCARDS time series. The green shaded areas indicates the root mean square uncertainty of the combined ~~datasets~~ data sets for each bin in SWOOSH data (σ_{rmss} in Davis et al. (2016)). Overall, there is a good agreement between the ML-TOMCAT, GOZCARDS and SWOOSH time series. As seen in Figure 1, ML-TOMCAT shows significant improvements in the tropical stratosphere compared to TOMCAT.

A peculiar detail of Figure 4 is that the standard deviation in the SWOOSH time series is largest during the 1991-1999 time period, which could be due to a combination of various factors. First, ~~for this time period, SWOOSH largely relies on~~ UARS MLS ozone profiles ~~. As UARS was launched in a near-circular orbit, the MLS latitudinal coverage was either 34°S – 80°N or 34°N – 80°S, depending on the spacecraft yaw position which alternated every 36 days (Barath et al., 1993) . Hence, for lower latitude ozone profiles during 1990s, SWOOSH relies on SAGE II and HALOE profiles with a low spatial sampling. Second, UARS MLS ozone profiles~~ are retrieved at only six levels per pressure decade (Livesey et al., 2003) instead of 12 levels per decade for Aura MLS (see https://mls.jpl.nasa.gov/data/v5-0_data_quality_document.pdf). ~~Third~~Second, significant enhancement in the stratospheric aerosol loading following the Mt. Pinatubo eruption in June 1991 ~~,~~ led to larger retrieval errors. Even with those uncertainties in SWOOSH (and GOZCARDS), ML-TOMCAT is generally close to the satellite-based ~~datasets~~ data sets for the entire time period and the agreement with satellite data is greatly improved in comparison ~~with~~ to the original TOMCAT ~~model~~ profile data. Supplementary Figures S1 to S10 also show an excellent agreement between ML-TOMCAT and the GOZCARDS/SWOOSH ~~datasets~~data sets for other latitude bands.

~~As discussed above, the ML-TOMCAT training dataset (SWOOSH) has large uncertainties in the 1990s.~~ Next we scrutinise percentage differences between GOZCARDS and ML-TOMCAT on the same pressure levels. Figure 5 shows relative differences between TOMCAT, ML-TOMCAT and SWOOSH ozone time series with respect to GOZCARDS. As seen earlier, TOMCAT ozone shows up to 40% positive biases in the lower stratosphere and 10% negative biases in the upper stratosphere (also seen in Figure 1). In contrast, ML-TOMCAT biases are well below 5% at all levels. At 50 hPa, TOMCAT biases seems to follow QBO-type oscillations that are correctly removed in ML-TOMCAT. Similarly, at 1 hPa TOMCAT differences show some uneven variations that could be linked to the inhomogeneities in the ERA-5 dynamical fields that are used to force TOMCAT. Furthermore, ML-TOMCAT differences show much smaller and almost linear biases at 1 hPa and lie well within the spread of GOZCARDS data.

Interestingly, although both GOZCARDS and SWOOSH are created by merging nearly identical ~~datasets~~data sets, there are differences between them which are largest for the 1984 to 2004 time period. This indicates that even slight differences in merging ~~methods~~ methodology leads to large differences in the merged ~~dataset~~data set. Although we use completely independent output from a CTM as a basis ~~dataset,~~ data set, GOZCARDS-ML-TOMCAT~~differences are not significantly different to SWOOSH differences~~ differences are within the expected discrepancy between GOZCARDS and SWOOSH data sets, especially at 10 and 50 hPa.

Another notable feature in Figure 5 is that at 50 hPa ~~,~~ ML-TOMCAT shows largest differences during 2020, which could be associated with the biases in ERA-5 dynamics during that period. A TOMCAT sensitivity simulation forced with ECMWF operational analysis data shows better agreement with MLS ozone variation during this period ~~(not shown)~~(e.g. Chrysanthou et al., 2021) . In addition, larger differences seen during 1984 (50 hPa), 1988 (10 hPa) and 1996-1999 (1 hPa) are most probably associated with SAGE II sampling issues and/or inhomogeneities in ERA-5 dynamical fields. However, a detailed analysis of these biases is out of scope of this study and it needs further investigation.

4.3.2 ~~Comparison with height level data~~

~~In this section, we~~

4.3.2 Comparison with altitude level data

We now compare ML-TOMCAT ozone profiles against ~~height-based merged satellite datasets~~altitude-based merged satellite data sets. Figure 6 shows ~~relative difference~~ the relative differences between TOMCAT/ML-TOMCAT vs SAGE-CCI-OMPS (Sofieva et al., 2017), BSVert (Hassler et al., 2018a) as well as SCIA-OMPS ~~(Arosio et al., 2018) datasets~~ (Arosio et al., 2019) data sets as a function of altitude and latitude. The top panels (a and b) compare the mean relative ~~difference~~ differences between the SAGE-CCI-OMPS ~~dataset~~data set, TOMCAT and ML-TOMCAT, respectively. Here TOMCAT shows large positive biases (up to 20%) in the lowermost stratosphere and negative biases (up to 15%) in the upper stratosphere. On the other hand, ML-TOMCAT shows only ±10% biases throughout the stratosphere. Larger biases are seen in the Antarctic stratosphere that could be attributed to the limited observational ozone profiles used to construct the ~~height-based~~ altitude-based merged satellite data products. Interestingly, ML-TOMCAT shows largest biases (up to 30%) w.r.t. the BSVert data set, though TOMCAT profiles (forced with ERA-Interim) are used ~~to construct the BSVert data set~~ as transfer function while constructing BSVert (Hassler et al., 2018a). In addition, in the lowermost stratosphere, biases are negative in the ~~SH latitudes and positive biases~~ tropics and SH mid-latitudes and positive in the NH mid-high latitudes. Hence, a contributing factor for these hemispherically asymmetric biases with respect to BSVert ozone profiles might be differences between ERA-Interim and ERA-5 reanalysis data (e.g. Ploeger et al., 2021) that are used to force these two ~~datasets. The strong~~ data sets. The negative values in relative differences in the lower tropical stratosphere shown with respect to the SCIA-OMPS ~~dataset~~ data set in the fourth panel ~~,~~ is systematic throughout the time series and is thought to be related to ~~the~~ two factors. The first one is the rather coarse vertical grid (corresponding to SCIAMACHY vertical resolution of 3.3 km) ~~and the merging methodology implemented. In the~~ which makes it sensitive to the interpolation onto the TOMCAT grid. The second is the difference in use of merging procedure implemented for SCIA-OMPS ~~dataset, no anomalies were computed, but OMPS was adjusted to SCIAMACHY mean values in each bin by using Aura MLS as a transfer function.~~and SWOOSH, so that ML-TOMCAT, trained over the MLS period using SWOOSH, shows a negative bias w.r.t. SCIA-OMPS, which however does not show such bias w.r.t. MLS (Arosio et al., 2019) .

Figure 7 compares TOMCAT and ML-TOMCAT profiles with the three ~~height-based ozone datasets~~ altitude-based ozone data sets with a focus on the equator (0° latitude). Supplementary Figures S11 to S20 show similar comparisons for 15°N, 15°S, 30°N, 30°S, 45°N, 45°S, 60°N, 60°S, 75°N, and 75°S latitude bins. Figure 8 displays the respective relative differences with respect to the SAGE-CCI-OMPS ~~dataset~~ data set which in this case is taken as a reference. In this way it is possible to evaluate the improvement introduced by applying the ML algorithm but also have an estimation of the discrepancies between different merged ~~datasets~~data sets, which is expected to be on the order of 5-10%. With respect to the comparison with the ~~datasets~~ data sets on pressure vertical coordinate, the scatter between the time series is larger here, due to the larger variety of different satellites available to produce the merged products and the fact that they have not been used in the ML training.

At about 45km in the tropics the ML algorithm seems to over-correct the negative bias shown by TOMCAT, leading to generally higher ozone values with respect to the other ~~datasets~~data sets, especially in the first half of the time series. In the middle stratosphere we find the best agreement between SAGE-CCI-OMPS and ML-TOMCAT; here the expected discrepancies among the merged ~~datasets~~ data sets are comparable to the differences observed between ML-TOMCAT and SAGE-CCI-OMPS. At the peak of the ozone number profile around 25 km, we notice generally lower values for ML-TOMCAT, on average by 5%. Similar biases are observed at mid-high latitude as well as seen in Supplementary Figures S11 to S20. The strong seasonal cycle seen in the TOMCAT difference with respect to the merged ~~datasets~~ data sets is largely reduced by ML-TOMCAT at this altitude.

4.3.3 Polar regions

The use of ML-TOMCAT helps to fill the observational gaps especially in atmospheric regions with lack of observations and before the beginning of the 21st century, when satellite measurements were sparser. For example, polar regions during local winter cannot be observed by limb observations based on scattered sunlight. Instruments such as Aura MLS and the Sounding of the Atmosphere using Broadband Emission Radiometry (SABER, Rong et al., 2008) ~~are generally~~ have generally been used to fill this gap over the last two decades. ~~Also for~~ For chemical models, complexities are also associated with the denitrification and dehydration (or chlorine activation) schemes that determine heterogeneous ozone losses (Grooß et al., 2018). Though most of our earlier studies showed that TOMCAT is able simulate to polar ozone losses quite realistically (e.g. Feng et al., 2007; Chipperfield et al., 2015, 2017; Dhomse et al., 2019), some systematic biases in polar stratosphere were noted in ~~Feng et al. (2021); Weber et al. (2021)~~ Feng et al. (2021) and Weber et al. (2021) . Figure 9 compares ozone at 18 km over the ~~North Pole which also demonstrates~~ Arctic demonstrating the good agreement between ML-TOMCAT and MLS in this region ~~, both during~~ for both local summer and winter ~~. In the bottom panel ,~~ seasons. The bottom panel shows the ozone sub-column over the ~~South Pole~~ Antarctic (poleward of 70°S latitude) ~~intergrated~~ integrated between 12 and 20 km ~~,~~ for TOMCAT, ML-TOMCAT and MLS averaged over September-October months. The good agreement between MLS and ML-TOMCAT during the ozone hole period is observed for most of the years. ML-TOMCAT enables the reconstruction of the large ozone losses which occurred in the 1980s during a phase when ozone depleting substances were on a rapid rise before the implementation of the Montreal Protocol and their phase out.

5 Summary and Conclusions

Stratospheric ozone concentrations are affected by many short- and long-term processes, hence high quality ozone profile ~~datasets~~ data sets are needed for accurate attribution studies. Though satellite instruments provide global measurements, due to their short mission durations various merging methodologies have been adopted to create homogeneous and gap-free long-term ozone profile ~~datasets~~data sets. Individual merging methodologies have distinct advantages and disadvantages. Atmospheric chemical models are also able to simulate chemically consistent long-term ~~datasets~~data sets, but they are prone to the deficiencies associated with the simplified parameterisations and uncertain parameters.

Here we have used TOMCAT CTM ozone profiles and a ~~RF~~ Random Forest (RF) regression model to create gap-free ozone profile ~~dataset~~ data set (ML-TOMCAT) for 1979-2020. The RF is ~~trained for~~ applied to the ozone difference between the SWOOSH and TOMCAT ozone profiles by selecting 20 years of MLS ~~measurement time periods~~ measurements (UARS-MLS and AURA-MLS) as a training period. RF show consistent performance throughout the stratosphere, except at high latitudes and the mid-latitude mid-stratosphere. Overall, ML-TOMCAT shows excellent agreement with SWOOSH for the entire time period (1984–2020), though somewhat larger differences are ~~visible~~ apparent for the period where limited ozone measurements are available for SWOOSH construction. We also find that ML-TOMCAT shows better agreement with satellite-based merged ~~datasets~~ data sets which use pressure as the vertical coordinate (e.g. SWOOSH, GOZCARDS) but weaker agreement with the ~~datasets which use height~~ data sets which use altitude (e.g. SAGE–CCI–OMPS, SCIA-OMPS). We find that at almost all stratospheric levels ML-TOMCAT ozone concentrations are well within uncertainties ~~in the observational datasets. The~~ of the observational data sets. TOMCAT ozone profiles outside the 316 – 1 hPa range can be considered as (slightly modified) TOMCAT profiles. For the next version of ML-TOMCAT~~dataset is thus~~, we aim at correcting tropospheric ozone profile biases using merged tropospheric ozone profile data sets described in Tropospheric Ozone Assessment Report (TOAR). Presently, the ML-TOMCAT V1.0 data set is ideally suited for the evaluation of chemical model ozone profiles from the tropopause to 0.1 hPa. ML-TOMCAT V1.0 ~~data~~ ozone profile data on pressure and altitude levels in mixing ratios and number density units is publicly available via https://zenodo.org/record/4997959#.YNzleUlKiUk.

Data availability. We thank Sean Davies for SWOOSH data which is publicly available via https://csl.noaa.gov/groups/csl8/swoosh/. We also thank Lucien Froidevaux (Lucien.Froidevaux@jpl.nasa.gov) for GOZCARDS v2 data. SAGE–CCI–OMPS was obtained via http://www.esa-ozone-cci.org. SCIA-OMPS data is available upon email request to AR or MW. BSVert data were obtained from https://zenodo.org/record/1217184 (Hassler et al., 2018b) . ML-TOMCAT V1.0 data is publicly available via https://zenodo.org/record/#.YNzleUlKiUk (Dhomse et al., 2021)

Acknowledgements. SD was supported by the NERC SISLAC project (NE/R001782/1). The financial support of part of this work from the State of Bremen, DAAD grant (CA), and ESA SOLVE Living Planet Fellowship (CA) is gratefully acknowledged. The UB contribution also benefited from the DFG VolImpact and BMBF SynopSys Projects. We thank NASA, NOAA and ESA for GOZCARDS, SWOOSH and SAGE-CCI-OMPS data products. We thank the European Centre for Medium-Range Weather Forecasts for providing their analyses. ~~The model~~ TOMCAT simulations were performed on the UK national Archer and Leeds Arc4 HPC systems.

References

Abalos, M. and de la Cámara, A.: Twenty-First Century Trends in Mixing Barriers and Eddy Transport in the Lower Stratosphere, Geophysical Research Letters, 47, e2020GL089 548, 2020.

Anderson, J., Russell Iii, J., Solomon, S., and Deaver, L.: Halogen Occultation Experiment confirmation of stratospheric chlorine decreases in accordance with the Montreal Protocol, Journal of Geophysical Research: Atmospheres, 105, 4483–4490, 2000.

Arosio, C., Rozanov, A., Malinina, E., Eichmann, K.-U., von Clarmann, T., and Burrows, J. P.: Retrieval of ozone profiles from OMPS limb scattering observations, Atmospheric Measurement Techniques, 11, 2135–2149, https://doi.org/10.5194/amt-11-2135-2018, 2018.

Arosio, C., Rozanov, A., Malinina, E., Weber, M., and Burrows, J. P.: Merging of ozone profiles from SCIAMACHY, OMPS and SAGE II observations to study stratospheric ozone changes, Atmospheric Measurement Techniques, 12, 2423–2444, https://doi.org/10.5194/amt-12-2423-2019, 2019.

Ball, W. T., Alsing, J., Mortlock, D. J., Staehelin, J., Haigh, J. D., Peter, T., Tummon, F., Stübi, R., Stenke, A., Anderson, J., Bourassa, A., Davis, S. M., Degenstein, D., Frith, S., Froidevaux, L., Roth, C., Sofieva, V., Wang, R., Wild, J., Yu, P., Ziemke, J. R., and Rozanov, E. V.: Evidence for a continuous decline in lower stratospheric ozone offsetting ozone layer recovery, Atmospheric Chemistry and Physics, 18, 1379–1394, https://doi.org/10.5194/acp-18-1379-2018, 2018.

Ball, W. T., Chiodo, G., Abalos, M., Alsing, J., and Stenke, A.: Inconsistencies between chemistry–climate models and observed lower stratospheric ozone trends since 1998, Atmospheric Chemistry and Physics, 20, 9737–9752, https://doi.org/10.5194/acp-20-9737-2020, 2020.

Barath, F. T., Chavez, M. C., Cofield, R. E., Flower, D. A., Frerking, M. A., Gram, M. B., Harris, W. M., Holden, J. R., Jarnot, R. F., Kloezeman, W. G., Klose, G. J., Lau, G. K., Loo, M. S., Maddison, B. J., Mattauch, R. J., McKinney, R. P., Peckham, G. E., Pickett, H. M., Siebes, G., Soltis, F. S., Suttie, R. A., Tarsala, J. A., Waters, J. W., and Wilson, W. J.: The Upper Atmosphere Research Satellite microwave limb sounder instrument, Journal of Geophysical Research: Atmospheres, 98, 10 751–10 762, https://doi.org/https://doi.org/10.1029/93JD00798, 1993.

Bernath, P. F., McElroy, C. T., Abrams, M. C., Boone, C. D., Butler, M., Camy-Peyret, C., Carleer, M., Clerbaux, C., Coheur, P.-F., Colin, R., DeCola, P., DeMazière, M., Drummond, J. R., Dufour, D., Evans, W. F. J., Fast, H., Fussen, D., Gilbert, K., Jennings, D. E., Llewellyn, E. J., Lowe, R. P., Mahieu, E., McConnell, J. C., McHugh, M., McLeod, S. D., Michaud, R., Midwinter, C., Nassar, R., Nichitiu, F., Nowlan, C., Rinsland, C. P., Rochon, Y. J., Rowlands, N., Semeniuk, K., Simon, P., Skelton, R., Sloan, J. J., Soucy, M.-A., Strong, K., Tremblay, P., Turnbull, D., Walker, K. A., Walkty, I., Wardle, D. A., Wehrle, V., Zander, R., and Zou, J.: Atmospheric Chemistry Experiment (ACE): Mission overview, Geophysical Research Letters, 32, https://doi.org/https://doi.org/10.1029/2005GL022386, 2005.

Bodeker, G., Hassler, B., Young, P., and Portmann, R. W.: A vertically resolved, global, gap-free ozone database for assessing or constraining global climate model simulations, Earth System Science Data, 5, 31–43, 2013.

Bognar, K., Alwarda, R., Strong, K., Chipperfield, M. P., Dhomse, S. S., Drummond, J. R., Feng, W., Fioletov, V., Goutail, F., Herrera, B., Manney, G. L., McCullough, E. M., Millán, L. F., Pazmino, A., Walker, K. A., Wizenberg, T., and Zhao, X.: Unprecedented Spring 2020 Ozone Depletion in the Context of 20 Years of Measurements at Eureka, Canada, Journal of Geophysical Research: Atmospheres, 126, e2020JD034 365, https://doi.org/https://doi.org/10.1029/2020JD034365, e2020JD034365 2020JD034365, 2021.

Bovensmann, H., Burrows, J., Buchwitz, M., Frerick, J., Noël, S., Rozanov, V., Chance, K., and Goede, A.: SCIAMACHY: Mission objectives and measurement modes, Journal of the atmospheric sciences, 56, 127–150, 1999.

Brasseur, G. P. and Solomon, S.: Aeronomy of the middle atmosphere: Chemistry and physics of the stratosphere and mesosphere, vol. 32, Springer Science & Business Media, 2006.

Breiman, L.: Random forests, Machine learning, 45, 5–32, 2001.

Carpenter, L. J., Daniel, J. S., Fleming, E. L., Hanaoka, T., Ju, H., Ravishankara, A. R., Ross, M. N., Tilmes, S., Wallington, T. J., and Wuebbles, D. J.: Scenarios and information for policy makers, in: Scientific Assessment of Ozone Depletion: 2018, World Meteorological Organization, Global Ozone Research and Monitoring Project - Report No. 58, chap. 6, World Meteorological Organization/UNEP, https://public.wmo.int/en/resources/library/scientific-assessment-of-ozone-depletion-2018, 2018.

Chipperfield, M. P.: New version of the TOMCAT/SLIMCAT off-line chemical transport model: Intercomparison of stratospheric tracer experiments, Quarterly Journal of the Royal Meteorological Society, 132, 1179–1203, https://doi.org/10.1256/qj.05.51, 2006.

Chipperfield, M. P., Dhomse, S. S., Feng, W., McKenzie, R. L., Velders, G. J. M., and Pyle, J. A.: Quantifying the ozone and ultraviolet benefits already achieved by the Montreal Protocol., Nature communications, 6, 7233, https://doi.org/10.1038/ncomms8233, 2015.

Chipperfield, M. P., Bekki, S., Dhomse, S., Harris, N. R. P., Hassler, B., Hossaini, R., Steinbrecht, W., Thiéblemont, R., and Weber, M.: Detecting recovery of the stratospheric ozone layer, Nature, 549, 211–218, https://doi.org/10.1038/nature23681, 2017.

Chipperfield, M. P., Dhomse, S., Hossaini, R., Feng, W., Santee, M. L., Weber, M., Burrows, J. P., Wild, J. D., Loyola, D., and Coldewey-Egbers, M.: On the Cause of Recent Variations in Lower Stratospheric Ozone, Geophysical Research Letters, 45, 5718–5726, https://doi.org/10.1029/2018GL078071, 2018.

Chrysanthou, A., Dhomse, S., Feng, W., Yajun, L., Hossaini, R., Ball, W., and Chipperfield, M.: The conundrum of the recent variations in the lower stratospheric ozone: An update, Quadrennial Ozone Symposium, pp. XX–XX, 2021.

Cionni, I., Eyring, V., Lamarque, J.-F., Randel, W., Stevenson, D., Wu, F., Bodeker, G., Shepherd, T., Shindell, D., and Waugh, D.: Ozone database in support of CMIP5 simulations: results and corresponding radiative forcing, Atmospheric Chemistry and Physics, 11, 11 267–11 292, 2011.

Coddington, O., Lean, J. L., Pilewskie, P., Snow, M., and Lindholm, D.: A solar irradiance climate data record, Bulletin of the American Meteorological Society, 97, 1265–1282, https://doi.org/10.1175/BAMS-D-14-00265.1, 2016.

Damadeo, R., Petropavlovskikh, I., Godin-Beekmann, S., Hubert, D., Sofieva, V., and Hassler, B.: The Long-term Ozone Trends and Uncertainties in the Stratosphere (LOTUS) SPARC activity: Lessons Learned, in: EGU General Assembly Conference Abstracts, p. 9953, 2018.

Damadeo, R. P., Zawodny, J. M., Thomason, L. W. L., and Iyer, N.: SAGE version 7.0 algorithm: application to SAGE II, Atmospheric Measurement Techniques, 6, 3539–3561, https://doi.org/10.5194/amt-6-3539-2013, 2013.

Davis, S. M., Rosenlof, K. H., Hassler, B., Hurst, D. F., Read, W. G., Vömel, H., Selkirk, H., Fujiwara, M., and Damadeo, R.: The Stratospheric Water and Ozone Satellite Homogenized (SWOOSH) database: a long-term database for climate studies, Earth System Science Data, 8, 461–490, https://doi.org/10.5194/essd-8-461-2016, 2016.

Dhomse, S., Weber, M., Wohltmann, I., Rex, M., and Burrows, J. P.: On the possible causes of recent increases in northern hemispheric total ozone from a statistical analysis of satellite data from 1979 to 2003, Atmospheric chemistry and physics, 6, 1165–1180, https://doi.org/10.5194/acp-6-1165-2006, 2006.

Dhomse, S., Feng, W., Montzka, S. A., Hossaini, R., Keeble, J., Pyle, J., Daniel, J., and Chipperfield, M.: Delay in recovery of the Antarctic ozone hole from unexpected CFC-11 emissions, Nature communications, 10, 1–12, 2019.

Dhomse, S. S., Chipperfield, M. P., Feng, W., Ball, W. T., Unruh, Y. C., Haigh, J. D., Krivova, N. A., Solanki, S. K., and Smith, A. K.: Stratospheric O3 changes during 2001—2010: the small role of solar flux variations in a chemical transport model, Atmospheric Chemistry and Physics, 13, 10 113–10 123, https://doi.org/10.5194/acp-13-10113-2013, 2013.

Dhomse, S. S., Chipperfield, M. P., Feng, W., Hossaini, R., Mann, G. W., and Santee, M. L.: Revisiting the hemispheric asymmetry in midlatitude ozone changes following the Mount Pinatubo eruption: A 3-D model study, Geophysical Research Letters, 42, 3038–3047, https://doi.org/10.1002/2015GL063052, 2015.

Dhomse, S. S., Chipperfield, M. P., Damadeo, R. P., Zawodny, J. M., Ball, W. T., Feng, W., Hossaini, R., Mann, G. W., and Haigh, J. D.: On the ambiguous nature of the 11-year solar cycle signal in upper stratospheric ozone, Geophysical Research Letters, 43, 7241–7249, https://doi.org/10.1002/2016GL069958, 2016.

Dhomse, S. S., Kinnison, D., Chipperfield, M. P., Salawitch, R. J., Cionni, I., Hegglin, M. I., Abraham, N. L., Akiyoshi, H., Archibald, A. T., Bednarz, E. M., Bekki, S., Braesicke, P., Butchart, N., Dameris, M., Deushi, M., Frith, S., Hardiman, S. C., Hassler, B., Horowitz, L. W., Hu, R.-M., Jöckel, P., Josse, B., Kirner, O., Kremser, S., Langematz, U., Lewis, J., Marchand, M., Lin, M., Mancini, E., Marécal, V., Michou, M., Morgenstern, O., O'Connor, F. M., Oman, L., Pitari, G., Plummer, D. A., Pyle, J. A., Revell, L. E., Rozanov, E., Schofield, R., Stenke, A., Stone, K., Sudo, K., Tilmes, S., Visioni, D., Yamashita, Y., and Zeng, G.: Estimates of ozone return dates from Chemistry-Climate Model Initiative simulations, Atmospheric Chemistry and Physics, 18, 8409–8438, https://doi.org/10.5194/acp-18-8409-2018, 2018.

Dhomse, S. S., Chipperfield, M. P., Feng, W., Arosio, C., Weber, M., and Rozanov, A.: ML-TOMCAT V1.0: Machine-Learning-Based Satellite- Corrected Global Stratospheric Ozone Profile Dataset, https://doi.org/10.5281/zenodo.4997959, 2021.

Errera, Q., Chabrillat, S., Christophe, Y., Debosscher, J., Hubert, D., Lahoz, W., Santee, M. L., Shiotani, M., Skachko, S., Clarmann, T. v., et al.: Reanalysis of Aura MLS chemical observations, Atmospheric Chemistry and Physics, 19, 13 647–13 679, 2019.

Feng, L., Brugge, R., Hólm, E., Harwood, R., O'Neill, A., Filipiak, M., Froidevaux, L., and Livesey, N.: Four-dimensional variational assimilation of ozone profiles from the Microwave Limb Sounder on the Aura satellite, Journal of Geophysical Research: Atmospheres, 113, 2008.

Feng, W., Chipperfield, M. P., Davies, S., von der Gathen, P., Kyrö, E., Volk, C. M., Ulanovsky, A., and Belyaev, G.: Large chemical ozone loss in 2004/2005 Arctic winter/spring, Geophysical Research Letters, 34, https://doi.org/10.1029/2006GL029098, 2007.

Feng, W., Dhomse, S. S., Arosio, C., Weber, M., Burrows, J. P., Santee, M. L., and Chipperfield, M. P.: Arctic ozone depletion in 2019/20: Roles of chemistry, dynamics and the Montreal Protocol, Geophysical Research Letters, https://doi.org/10.1029/2020GL091911, 2021.

Froidevaux, L., Livesey, N., Read, W., Salawitch, R., Waters, J., Drouin, B., MacKenzie, I., Pumphrey, H., Bernath, P., Boone, C., et al.: Temporal decrease in upper atmospheric chlorine, Geophysical Research Letters, 33, 2006a.

Froidevaux, L., Livesey, N. J., Read, W. G., Jiang, Y. B., Jimenez, C., Filipiak, M. J., Schwartz, M. J., Santee, M. L., Pumphrey, H. C., Jiang, J. H., et al.: Early validation analyses of atmospheric profiles from EOS MLS on the Aura satellite, IEEE Transactions on Geoscience and Remote Sensing, 44, 1106–1121, 2006b.

Froidevaux, L., Anderson, J., Wang, H.-J., Fuller, R., Schwartz, M., Santee, M., Livesey, N., Pumphrey, H., Bernath, P., Russell III, J., et al.: Global OZone Chemistry And Related trace gas Data records for the Stratosphere (GOZCARDS): methodology and sample results with a focus on HCl, H 2 O, and O 3, Atmospheric Chemistry and Physics, 15, 10 471–10 507, 2015.

Froidevaux, L., Kinnison, D. E., Wang, R., Anderson, J., and Fuller, R. A.: Evaluation of CESM1 (WACCM) free-running and specified dynamics atmospheric composition simulations using global multispecies satellite data records, Atmospheric Chemistry and Physics, 19, 4783–4821, 2019.

Galytska, E., Rozanov, A., Chipperfield, M. P., Dhomse, Weber, M., Arosio, C., Feng, W., and Burrows, J. P.: Dynamically controlled ozone decline in the tropical mid-stratosphere observed by SCIAMACHY, Atmospheric Chemistry and Physics, 19, 767–783, https://doi.org/10.5194/acp-19-767-2019, 2019.

Ghosh, S., Pyle, J. A., and Good, P.: Temperature dependence of the ClO concentration near the stratopause, Journal of Geophysical Research: Atmospheres, 102, 19 207–19 216, https://doi.org/https://doi.org/10.1029/97JD01099, 1997.

Grooß, J.-U., Müller, R., Spang, R., Tritscher, I., Wegner, T., Chipperfield, M. P., Feng, W., Kinnison, D. E., and Madronich, S.: On the discrepancy of HCl processing in the core of the wintertime polar vortices, Atmospheric Chemistry and Physics, 18, 8647–8666, https://doi.org/10.5194/acp-18-8647-2018, 2018.

Haigh, J.: The role of stratospheric ozone in modulating the solar radiative forcing of climate, Nature, 370, 544–546, https://doi.org/https://doi.org/10.1038/370544a0, 1994.

Haigh, J., Winning, A., Toumi, R., and Harder, J.: An influence of solar spectral variations on radiative forcing of climate, Nature, 467, https://doi.org/https://doi.org/10.1038/370544a0, 2010.

Harrison, J. J., Chipperfield, M. P., Boone, C. D., Dhomse, S. S., and Bernath, P. F.: Fifteen Years of HFC-134a Satellite Observations: Comparisons With SLIMCAT Calculations, Journal of Geophysical Research: Atmospheres, 126, e2020JD033 208, https://doi.org/https://doi.org/10.1029/2020JD033208, e2020JD033208 2020JD033208, 2021.

Hassler, B., Bodeker, G., and Dameris, M.: A new global database of trace gases and aerosols from multiple sources of high vertical resolution measurements, Atmospheric Chemistry and Physics, 8, 5403–5421, 2008.

Hassler, B., Kremser, S., Bodeker, G. E., Lewis, J., Nesbit, K., Davis, S. M., Chipperfield, M. P., Dhomse, S. S., and Dameris, M.: An updated version of a gap-free monthly mean zonal mean ozone database, Earth System Science Data, 10, 1473–1490, 2018a.

Hassler, B., Stefanie, K., Greg, B., Jared, L., Kage, N., Sean, D., Martyn, C., Sandip, D., and Martin, D.: BSVerticalOzone database, https://doi.org/10.5281/zenodo.1217184, 2018b.

Hersbach, H., Bell, B., Berrisford, P., Hirahara, S., Horányi, A., Muñoz-Sabater, J., Nicolas, J., Peubey, C., Radu, R., Schepers, D., Simmons, A., Soci, C., Abdalla, S., Abellan, X., Balsamo, G., Bechtold, P., Biavati, G., Bidlot, J., Bonavita, M., De Chiara, G., Dahlgren, P., Dee, D., Diamantakis, M., Dragani, R., Flemming, J., Forbes, R., Fuentes, M., Geer, A., Haimberger, L., Healy, S., Hogan, R. J., Hólm, E., Janisková, M., Keeley, S., Laloyaux, P., Lopez, P., Lupu, C., Radnoti, G., de Rosnay, P., Rozum, I., Vamborg, F., Villaume, S., and Thépaut, J.-N.: The ERA5 global reanalysis, Quarterly Journal of the Royal Meteorological Society, 146, 1999–2049, https://doi.org/https://doi.org/10.1002/qj.3803, 2020.

Holton, J. R., Haynes, P. H., McIntyre, M. E., Douglass, A. R., Rood, R. B., and Pfister, L.: Stratosphere-troposphere exchange, Reviews of Geophysics, 33, 403–439, https://doi.org/10.1029/95RG02097, 1995.

Hossaini, R., Chipperfield, M. P., Montzka, S. A., Rap, A., Dhomse, S., and Feng, W.: Efficiency of short-lived halogens at influencing climate through depletion of stratospheric ozone, Nature Geoscience, advance on, 186–190, https://doi.org/10.1038/ngeo2363, 2015.

Hossaini, R., Atlas, E., Dhomse, S. S., Chipperfield, M. P., Bernath, P. F., Fernando, A. M., Mühle, J., Leeson, A. A., Montzka, S. A., Feng, W., Harrison, J. J., Krummel, P., Vollmer, M. K., Reimann, S., O'Doherty, S., Young, D., Maione, M., Arduini, J., and Lunder, C. R.: Recent Trends in Stratospheric Chlorine From Very Short-Lived Substances, Journal of Geophysical Research: Atmospheres, 124, 2318–2335, https://doi.org/10.1029/2018JD029400, 2019.

Kotsiantis, S. B.: Decision trees: a recent overview, Artificial Intelligence Review, 39, 261–283, 2013.

Li, Y., Chipperfield, M. P., Feng, W., Dhomse, S. S., Pope, R. J., Li, F., and Guo, D.: Analysis and attribution of total column ozone changes over the Tibetan Plateau during 1979–2017, Atmospheric Chemistry and Physics, 20, 8627–8639, https://doi.org/10.5194/acp-20-8627-2020, 2020.

Livesey, N. J., Read, W. G., Froidevaux, L., Waters, J. W., Santee, M. L., Pumphrey, H. C., Wu, D. L., Shippony, Z., and Jarnot, R. F.: The UARS Microwave Limb Sounder version 5 data set: Theory, characterization, and validation, Journal of Geophysical Research: Atmospheres, 108, https://doi.org/https://doi.org/10.1029/2002JD002273, 2003.

Livesey, N. J., Read, W. G., Wagner, P. A., Froidevaux, L., Santee, M. L., Schwartz, M. J., Lambert, A., Millan, L., Pumphrey, H. C., Manney, G. L., Fulle, r. R. A., Jarnot, R. F., Knosp, B. W., and Lay, R. R.: EOS MLS Version 5.0x Level 2 and 3 data quality and description document., Jet Propulsion Laboratory, California Institute of Technology, Pasadena, CA, 2020.

Luo, B.: Stratospheric aerosol data for use in CMIP6 models, ftp://iacftp.ethz.ch/pub{_}read/luo/CMIP6/Readme{_}Data{_}Description.pdf, 2016.

Mahieu, E., Chipperfield, M. P., Notholt, J., Reddmann, T., Anderson, J., Bernath, P. F., Blumenstock, T., Coffey, M. T., Dhomse, S. S., Feng, W., Franco, B., Froidevaux, L., Griffith, D. W. T., Hannigan, J. W., Hase, F., Hossaini, R., Jones, N. B., Morino, I., Murata, I., Nakajima, H., Palm, M., Paton-Walsh, C., Russell, J. M., Schneider, M., Servais, C., Smale, D., Walker, K. A., III, J. M. R., Schneider, M., Servais, C., Smale, D., and Walker, K. A.: Recent Northern Hemisphere stratospheric HCl increase due to atmospheric circulation changes, Nature, 515, 104–107, https://doi.org/10.1038/nature13857, 2014.

McCormick, M., Zawodny, J., Veiga, R., Larsen, J., and Wang, P.: An overview of SAGE I and II ozone measurements, Planetary and Space Science, 37, 1567–1586, 1989.

Millán, L. F., Livesey, N. J., Santee, M. L., Neu, J. L., Manney, G. L., and Fuller, R. A.: Case studies of the impact of orbital sampling on stratospheric trend detection and derivation of tropical vertical velocities: solar occultation vs. limb emission sounding, Atmospheric Chemistry and Physics, 16, 11 521–11 534, https://doi.org/10.5194/acp-16-11521-2016, 2016.

Mitchell, D. M., Lo, Y. E., Seviour, W. J., Haimberger, L., and Polvani, L. M.: The vertical profile of recent tropical temperature trends: Persistent model biases in the context of internal variability, Environmental Research Letters, 15, 1040b4, 2020.

Montzka, S. A., Dutton, G. S., Yu, P., Ray, E., Portmann, R. W., Daniel, J. S., Kuijpers, L., Hall, B. D., Mondeel, D., Siso, C., et al.: An unexpected and persistent increase in global emissions of ozone-depleting CFC-11, Nature, 557, 413–417, 2018.

Montzka, S. A., Dutton, G. S., Portmann, R. W., Chipperfield, M. P., Davis, S., Feng, W., Manning, A. J., Ray, E., Rigby, M., Hall, B. D., et al.: A decline in global CFC-11 emissions during 2018- 2019, Nature, pp. 1–5, 2021.

Murtagh, D., Frisk, U., Merino, F., Ridal, M., Jonsson, A., Stegman, J., Witt, G., Eriksson, P., Jiménez, C., Megie, G., de La Noë, J., Ricaud, P., Baron, P., Pardo, J. R., Hauchcorne, A., Llewellyn, E. J., Degenstein, D. A., Gattinger, R. L., Lloyd, N. D., Evans, W. F. J., McDade, I. C., Haley, C. S., Sioris, C., von Savigny, C., Solheim, B. H., McConnell, J. C., Strong, K., Richardson, E. H., Leppelmeier, G. W., Kyrölä, E., Auvinen, H., and Oikarinen, L.: Review: An overview of the Odin atmospheric mission, Canadian Journal of Physics, 80, 309–319, https://doi.org/10.1139/p01-157, 2002.

Orbe, C., Wargan, K., Pawson, S., and Oman, L. D.: Mechanisms linked to recent ozone decreases in the Northern Hemisphere lower stratosphere, Journal of Geophysical Research: Atmospheres, 125, e2019JD031 631, 2020.

Paul, J., Fortuin, F., and Kelder, H.: An ozone climatology based on ozonesonde and satellite measurements, Journal of Geophysical Research: Atmospheres, 103, 31 709–31 734, 1998.

Pedregosa, F., Varoquaux, G., Gramfort, A., Michel, V., Thirion, B., Grisel, O., Blondel, M., Prettenhofer, P., Weiss, R., Dubourg, V., et al.: Scikit-learn: Machine learning in Python, the Journal of machine Learning research, 12, 2825–2830, 2011.

Petropavlovskikh, I., Godin-Beekmann, S., Hubert, D., Damadeo, R., Hassler, B., and Sofieva, V.: SPARC/IO3C/GAW Report on Long-term Ozone Trends and Uncertainties in the Stratosphere, Tech. rep., SPARC, https://elib.dlr.de/126666/, 9th assessment report of the SPARC project, published by the International Project Office at DLR-IPA. also: GAW Report No. 241; WCRP Report 17/2018, 2019.

Ploeger, F., Diallo, M., Charlesworth, E., Konopka, P., Legras, B., Laube, J. C., Grooß, J.-U., Günther, G., Engel, A., and Riese, M.: The stratospheric Brewer–Dobson circulation inferred from age of air in the ERA5 reanalysis, Atmospheric Chemistry and Physics Discussions, 2021, 1–27, https://doi.org/10.5194/acp-2020-1253, 2021.

Prignon, M., Chabrillat, S., Friedrich, M., Smale, D., Strahan, S. E., Bernath, P. F., Chipperfield, M. P., Dhomse, S. S., Feng, W., Minganti, D., Servais, C., and Mahieu, E.: Stratospheric fluorine as a tracer of circulation changes: comparison between infrared remote-sensing observations and simulations with five modern reanalyses, Journal of Geophysical Research: Atmospheres, n/a, e2021JD034 995, https://doi.org/10.1029/2021JD034995, e2021JD034995 2021JD034995, 2021.

Rahpoe, N., Weber, M., Rozanov, A. V., Weigel, K., Bovensmann, H., Burrows, J. P., Laeng, A., Stiller, G., von Clarmann, T., Kyrölä, E., Sofieva, V. F., Tamminen, J., Walker, K., Degenstein, D., Bourassa, A. E., Hargreaves, R., Bernath, P., Urban, J., and Murtagh, D. P.: Relative drifts and biases between six ozone limb satellite measurements from the last decade, Atmospheric Measurement Techniques, 8, 4369–4381, https://doi.org/10.5194/amt-8-4369-2015, 2015.

Randel, W. J. and Wu, F.: A stratospheric ozone profile data set for 1979–2005: Variability, trends, and comparisons with column ozone data, Journal of Geophysical Research: Atmospheres, 112, 2007.

Rong, P., Russell III, J., Mlynczak, M., Remsberg, E., Marshall, B., Gordley, L., and Lopez-Puertas, M.: Validation of TIMED/SABER v1. 07 ozone at 9.6 μm in the altitude range 15–70km, J. Geophys. Res, 114, D04 306, 2008.

Russell III, J. M., Gordley, L. L., Park, J. H., Drayson, S. R., Hesketh, W. D., Cicerone, R. J., Tuck, A. F., Frederick, J. E., Harries, J. E., and Crutzen, P. J.: The halogen occultation experiment, Journal of Geophysical Research: Atmospheres, 98, 10 777–10 797, 1993.

Skachko, S., Errera, Q., Ménard, R., Christophe, Y., and Chabrillat, S.: Comparison of the ensemble Kalman filter and 4D-Var assimilation methods using a stratospheric tracer transport model, Geoscientific Model Development, 7, 1451–1465, https://doi.org/10.5194/gmd-7-1451-2014, 2014.

Sofieva, V. F., Kalakoski, N., Päivärinta, S.-M., Tamminen, J., Laine, M., and Froidevaux, L.: On sampling uncertainty of satellite ozone profile measurements, Atmospheric Measurement Techniques, 7, 1891–1900, https://doi.org/10.5194/amt-7-1891-2014, 2014.

Sofieva, V. F., Kyrölä, E., Laine, M., Tamminen, J., Degenstein, D., Bourassa, A., Roth, C., Zawada, D., Weber, M., Rozanov, A., Rahpoe, N., Stiller, G., Laeng, A., von Clarmann, T., Walker, K. A., Sheese, P., Hubert, D., van Roozendael, M., Zehner, C., Damadeo, R., Zawodny, J., Kramarova, N., and Bhartia, P. K.: Merged SAGE II, Ozone_cci and OMPS ozone profile dataset and evaluation of ozone trends in the stratosphere, Atmospheric Chemistry and Physics, 17, 12 533–12 552, https://doi.org/10.5194/acp-17-12533-2017, 2017.

Sofieva, V. F., Szeląg, M., Tamminen, J., Kyrölä, E., Degenstein, D., Roth, C., Zawada, D., Rozanov, A., Arosio, C., Burrows, J. P., Weber, M., Laeng, A., Stiller, G. P., von Clarmann, T., Froidevaux, L., Livesey, N., van Roozendael, M., and Retscher, C.: Measurement report: regional trends of stratospheric ozone evaluated using the MErged GRIdded Dataset of Ozone Profiles (MEGRIDOP), Atmospheric Chemistry and Physics, 21, 6707–6720, https://doi.org/10.5194/acp-21-6707-2021, 2021.

Solomon, S., Ivy, D. J., Kinnison, D., Mills, M. J., Neely, R. R., and Schmidt, A.: Emergence of healing in the Antarctic ozone layer, Science, http://science.sciencemag.org/content/early/2016/06/30/science.aae0061, 2016.

Steinbrecht, W., Froidevaux, L., Fuller, R., Wang, R., Anderson, J., Roth, C., Bourassa, A., Degenstein, D., Damadeo, R., Zawodny, J., Frith, S., McPeters, R., Bhartia, P., Wild, J., Long, C., Davis, S., Rosenlof, K., Sofieva, V., Walker, K., Rahpoe, N., Rozanov, A., Weber, M., Laeng, A., von Clarmann, T., Stiller, G., Kramarova, N., Godin-Beekmann, S., Leblanc, T., Querel, R., Swart, D., Boyd, I., Hocke, K., Kämpfer, N., Maillard Barras, E., Moreira, L., Nedoluha, G., Vigouroux, C., Blumenstock, T., Schneider, M., García, O., Jones, N., Mahieu, E., Smale, D., Kotkamp, M., Robinson, J., Petropavlovskikh, I., Harris, N., Hassler, B., Hubert, D., and Tummon, F.: An update on ozone profile trends for the period 2000 to 2016, Atmospheric Chemistry and Physics, 17, 10 675–10 690, https://doi.org/10.5194/acp-17-10675-2017, 2017.

Stolarski, R. S., Douglass, A. R., Newman, P. A., Pawson, S., and Schoeberl, M. R.: Relative Contribution of Greenhouse Gases and Ozone-Depleting Substances to Temperature Trends in the Stratosphere: A Chemistry–Climate Model Study, Journal of Climate, 23, 28–42, https://doi.org/10.1175/2009JCLI2955.1, 2010.

Strahan, S. E., Douglass, A. R., Stolarski, R. S., Akiyoshi, H., Bekki, S., Braesicke, P., Butchart, N., Chipperfield, M. P., Cugnet, D., Dhomse, S., Frith, S. M., Gettelman, A., Hardiman, S. C., Kinnison, D. E., Lamarque, J. F., Mancini, E., Marchand, M., Michou, M., Morgenstern, O., Nakamura, T., Olivie, D., Pawson, S., Pitari, G., Plummer, D. A., Pyle, J. A., Scinocca, J. F., Shepherd, T. G., Shibata, K., Smale, D., Teyssedre, H., Tian, W., and Yamashita, Y.: Using transport diagnostics to understand chemistry climate model ozone simulations, Journal of Geophysical ResearchAtmospheres, 116, https://doi.org/10.1029/2010jd015360, 2011.

Sukhodolov, T., Rozanov, E., Ball, W., Bais, A., Tourpali, K., Shapiro, A., Telford, P., Smyshlyaev, S., Fomin, B., Sander, R., Bossay, S., Bekki, S., Marchand, M., Chipperfield, M., Dhomse, S., Haigh, J., Peter, T., and Schmutz, W.: Evaluation of simulated photolysis rates and their response to solar irradiance variability, Journal of Geophysical Research: Atmospheres, 121, https://doi.org/10.1002/2015JD024277, 2016.

Svetnik, V., Liaw, A., Tong, C., Culberson, J. C., Sheridan, R. P., and Feuston, B. P.: Random forest: a classification and regression tool for compound classification and QSAR modeling, Journal of chemical information and computer sciences, 43, 1947–1958, 2003.

Szeląg, M. E., Sofieva, V. F., Degenstein, D., Roth, C., Davis, S., and Froidevaux, L.: Seasonal stratospheric ozone trends over 2000–2018 derived from several merged data sets, Atmospheric Chemistry and Physics, 20, 7035–7047, 2020.

Tian, W., Chipperfield, M. P., Gray, L. J., and Zawodny, J. M.: Quasi-biennial oscillation and tracer distributions in a coupled chemistry-climate model, Journal of Geophysical Research: Atmospheres, 111, https://doi.org/https://doi.org/10.1029/2005JD006871, 2006.

Wales, P. A., Salawitch, R. J., Nicely, J. M., Anderson, D. C., Canty, T. P., Baider, S., Dix, B., Koenig, T. K., Volkamer, R., Chen, D., Huey, L. G., Tanner, D. J., Cuevas, C. A., Fernandez, R. P., Kinnison, D. E., Lamarque, J.-F., Saiz-Lopez, A., Atlas, E. L., Hall, S. R., Navarro, M. A., Pan, L. L., Schauffler, S. M., Stell, M., Tilmes, S., Ullmann, K., Weinheimer, A. J., Akiyoshi, H., Chipperfield, M. P., Deushi, M., Dhomse, S. S., Feng, W., Graf, P., Hossaini, R., Jöckel, P., Mancini, E., Michou, M., Morgenstern, O., Oman, L. D., Pitari, G., Plummer, D. A., Revell, L. E., Rozanov, E., Saint-Martin, D., Schofield, R., Stenke, A., Stone, K., Visioni, D., Yamashita, Y., and Zeng, G.: Stratospheric Injection of Brominated Very Short-Lived Substances Inferred from Aircraft Observations of Organic Bromine and BrO in the Western Pacific, Journal of Geophysical Research: Atmospheres, 0, https://doi.org/10.1029/2017JD027978, 2018.

Wargan, K., Orbe, C., Pawson, S., Ziemke, J. R., Oman, L. D., Olsen, M. A., Coy, L., and Emma Knowland, K.: Recent decline in extratropical lower stratospheric ozone attributed to circulation changes, Geophysical research letters, 45, 5166–5176, 2018.

Wargan, K., Weir, B., Manney, G. L., Cohn, S. E., and Livesey, N. J.: The anomalous 2019 Antarctic ozone hole in the GEOS Constituent Data Assimilation System with MLS observations, Journal of Geophysical Research: Atmospheres, 125, e2020JD033 335, 2020.

Weber, M., Dhomse, S., Wittrock, F., Richter, A., Sinnhuber, B.-M., and Burrows, J. P.: Dynamical control of NH and SH winter/spring total ozone from GOME observations in 1995–2002, Geophysical Research Letters, 30, 1583, https://doi.org/10.1029/2002GL016799, 2003.

Weber, M., Dikty, S., Burrows, J. P., Garny, H., Dameris, M., Kubin, A., Abalichin, J., and Langematz, U.: The Brewer-Dobson circulation and total ozone from seasonal to decadal time scales, Atmospheric Chemistry and Physics, 11, 11 221–11 235, https://doi.org/10.5194/acp-11-11221-2011, 2011.

Weber, M., Arosio, C., Feng, W., Dhomse, S. S., Chipperfield, M. P., Meier, A., Burrows, J. P., Eichmann, K.-U., Richter, A., and Rozanov, A.: The Unusual Stratospheric Arctic Winter 2019/20: Chemical Ozone Loss From Satellite Observations and TOMCAT Chemical Transport Model, Journal of Geophysical Research: Atmospheres, 126, e2020JD034 386, https://doi.org/https://doi.org/10.1029/2020JD034386, e2020JD034386 2020JD034386, 2021.

WMO: Scientific Assessment of Ozone Depletion:2014, Tech. rep., World Meteorological Organization, Global Ozone Research and Monitoring Project, Report No. 55, Geneva, Switzerland, https://www.wmo.int/pages/prog/arep/gaw/ozone{_}2014/, 2014.

WMO: Scientific Assessment of Ozone Depletion:2018, Tech. rep., World Meteorological Organization, Global Ozone Research and Monitoring Project, Report No. 58, Geneva, Switzerland, https://www.wmo.int/pages/prog/arep/gaw/ozone{_}2018/, 2018.

Wohltmann, I., Gathen, P., Lehmann, R., Maturilli, M., Deckelmann, H., Manney, G. L., Davies, J., Tarasick, D., Jepsen, N., Kivi, R., Lyall, N., and Rex, M.: Near-complete local reduction of Arctic stratospheric ozone by severe chemical loss in spring 2020, Geophysical Research Letters, 47, https://doi.org/10.1029/2020GL089547, 2020.

Zawada, D. J., Rieger, L. A., Bourassa, A. E., and Degenstein, D. A.: Tomographic retrievals of ozone with the OMPS Limb Profiler: algorithm description and preliminary results, Atmospheric Measurement Techniques, 11, 2375–2393, https://doi.org/10.5194/amt-11-2375-2018, 2018.

Author contributions. SD conceived the idea and initiated the study in discussion with MPC. The model runs were performed and analysed by SD, MPC and WF. The figures were prepared by CA and SD. The paper was written by SD, MPC and MW who included comments from all of the other coauthors.

Competing interests. The authors have no competing interests

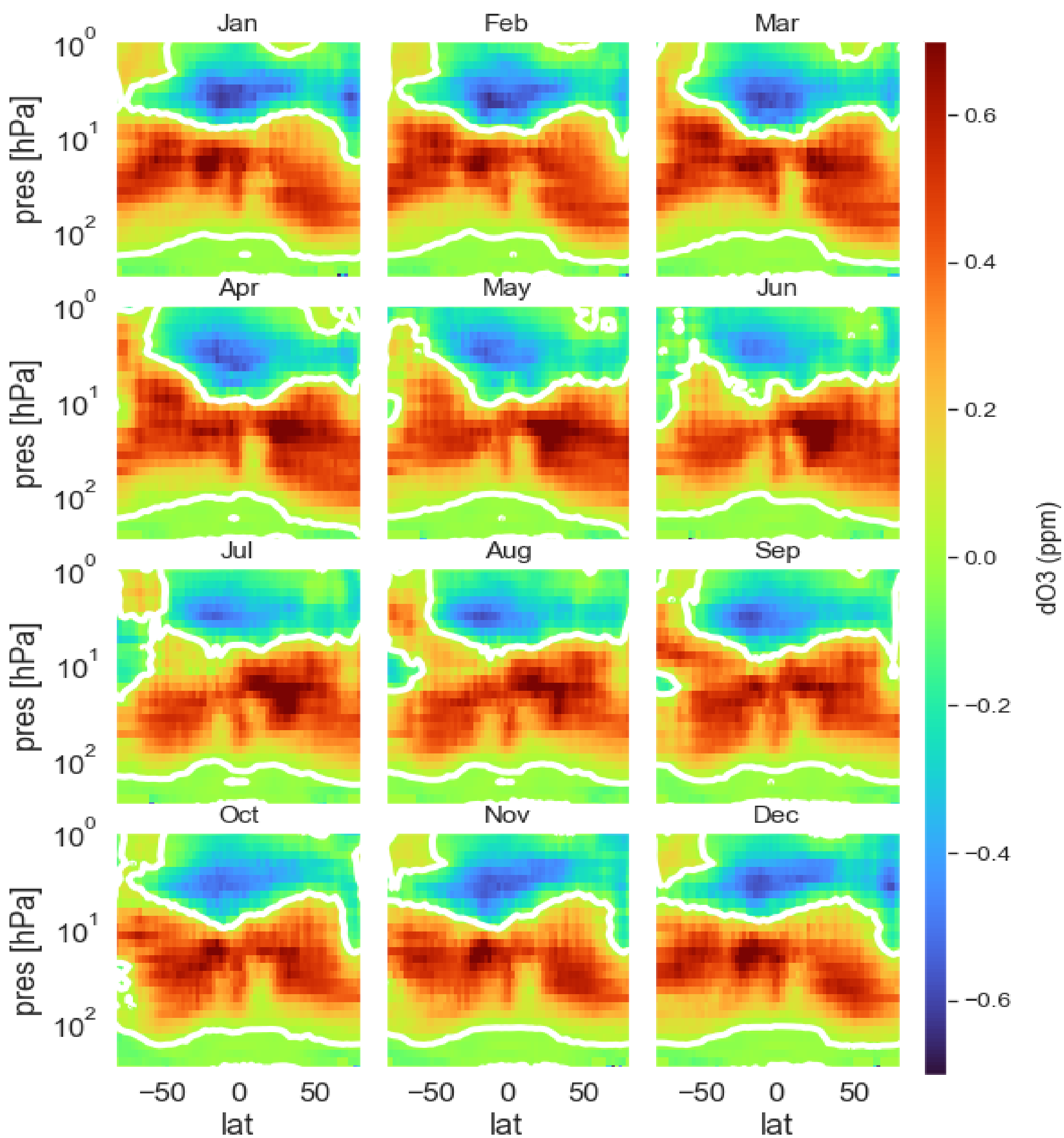

Figure 1. Latitude-pressure cross sections of the climatological (~~2001-2020~~2006-2020) monthly mean difference (ppm) between TOMCAT and SWOOSH (Davis et al., 2016) ~~and TOMCAT~~ ozone profiles.

o

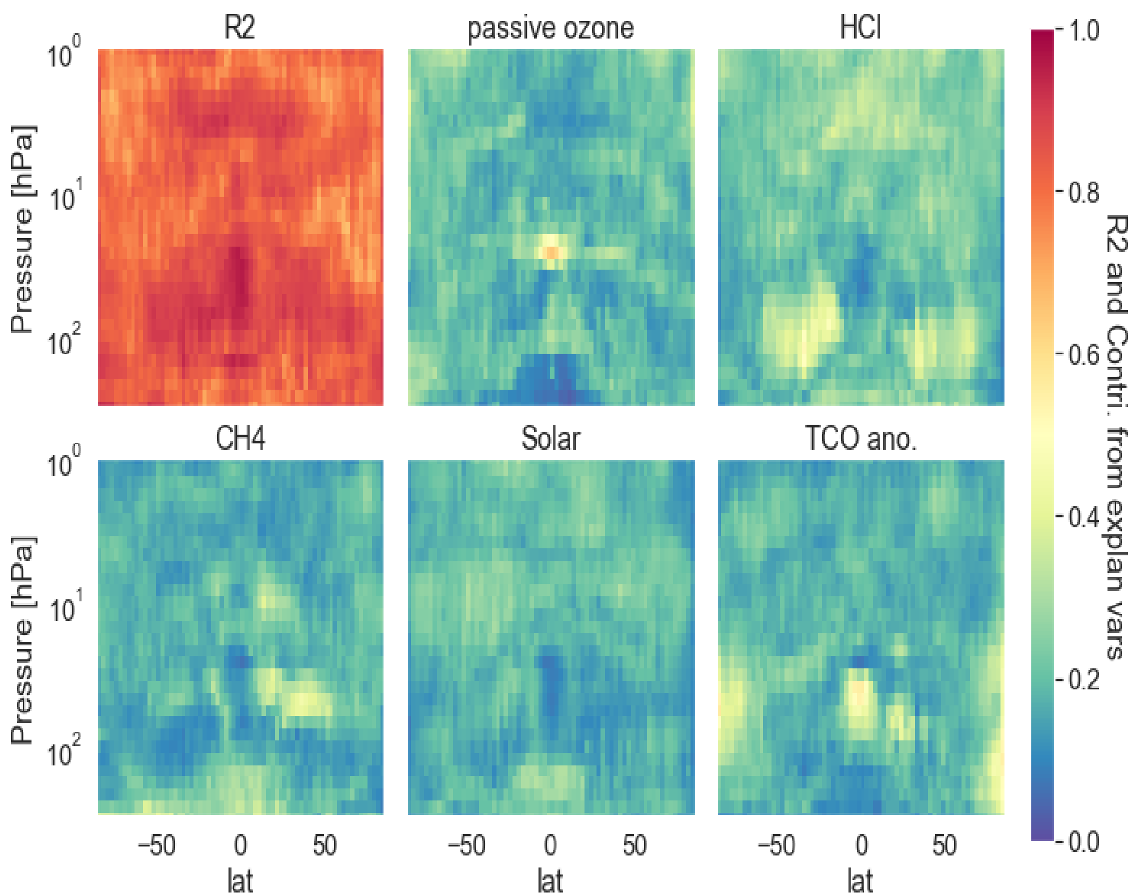

Figure 2. Latitude-pressure cross sections of the variance (R^2) and regression coefficients from passive ozone, ~~HCl~~HCl, ~~CH_4~~CH_4, solar and total column ozone anomaly (see main text equation 1).

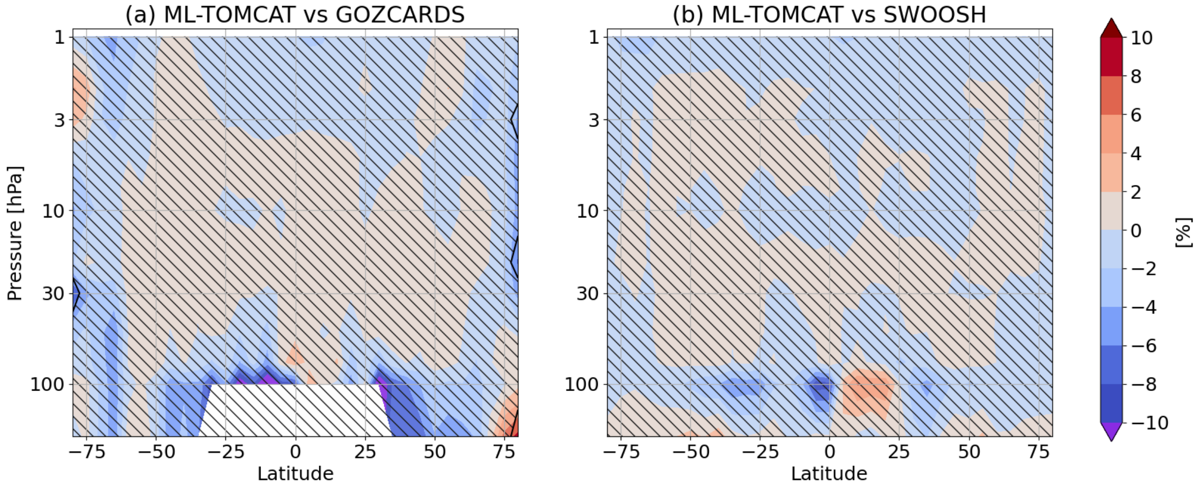

Figure 3. Relative differences (in percent) as a function of pressure and latitude between ML-TOMCAT and (a) GOZCARDS V2 (Froidevaux et al., 2019) and (b) SWOOSH (Davis et al., 2016). Stippling indicates regions where differences are statistically insignificant.

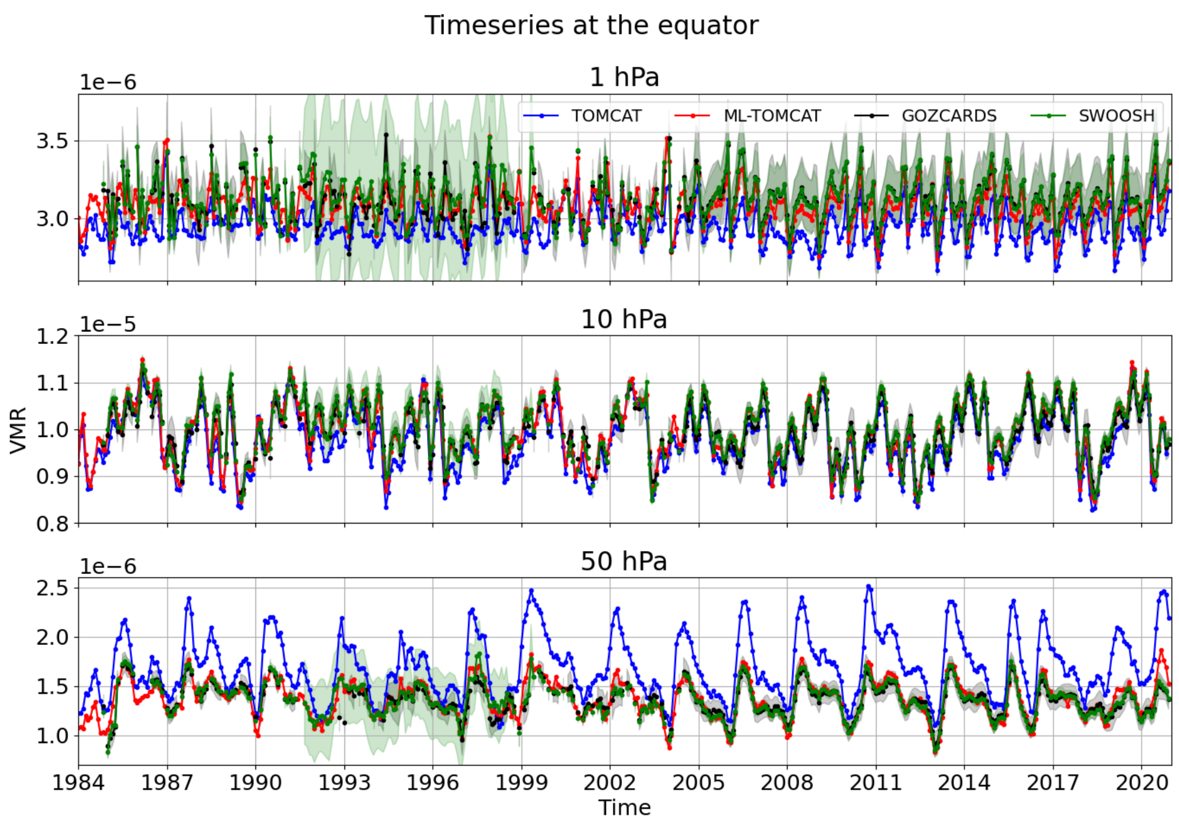

Figure 4. Comparison between TOMCAT (blue lines) and ML-TOMCAT (red lines) ozone mixing ratios over the equator (0°) at (a, top) 1 hPa, (b, middle) 10 hPa and (c, bottom) 50 hPa. Satellite-based ozone mixing ratios from GOZCARDS (Froidevaux et al., 2019) and SWOOSH (Davis et al., 2016) ~~datasets~~ data sets along with their uncertainty estimates (shaded) are shown with black and green coloured lines, respectively.

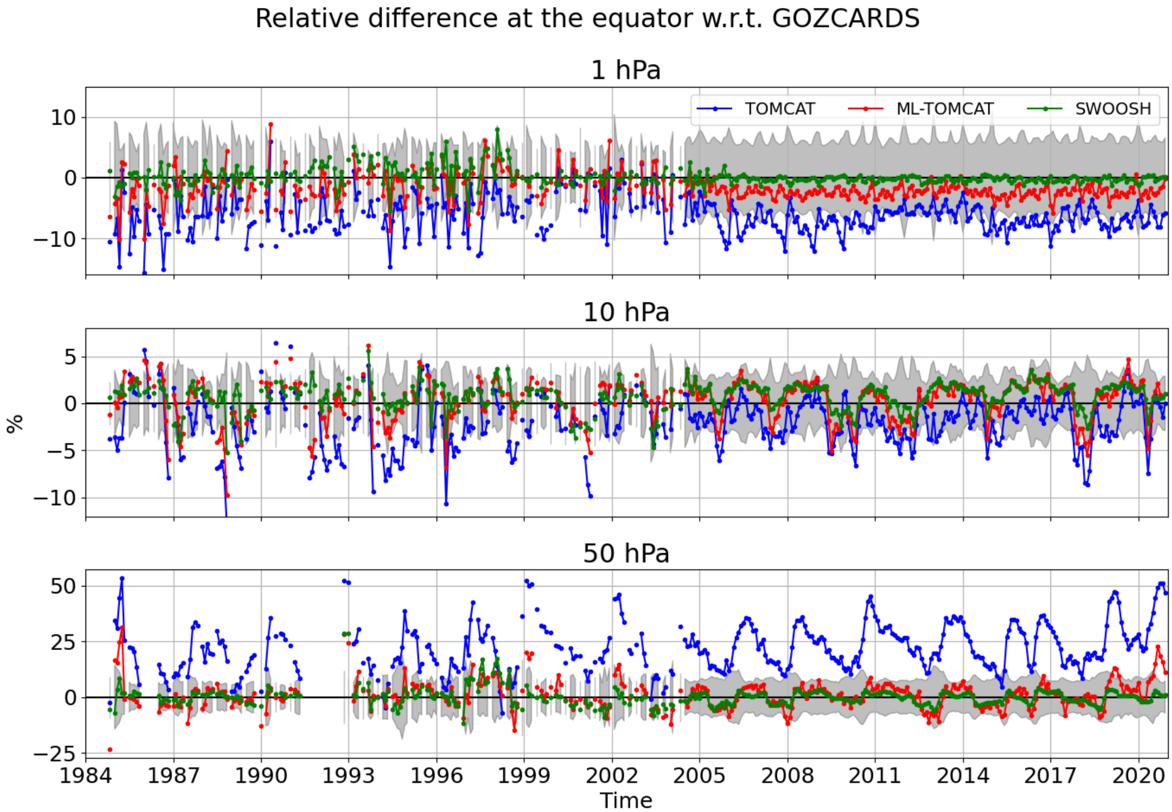

Figure 5. As Figure 4 but for the residuals, i.e. relative differences between SWOOSH (green), TOMCAT (blue) and ML-TOMCAT (red) ozone with respect to GOZCARDS ozone.

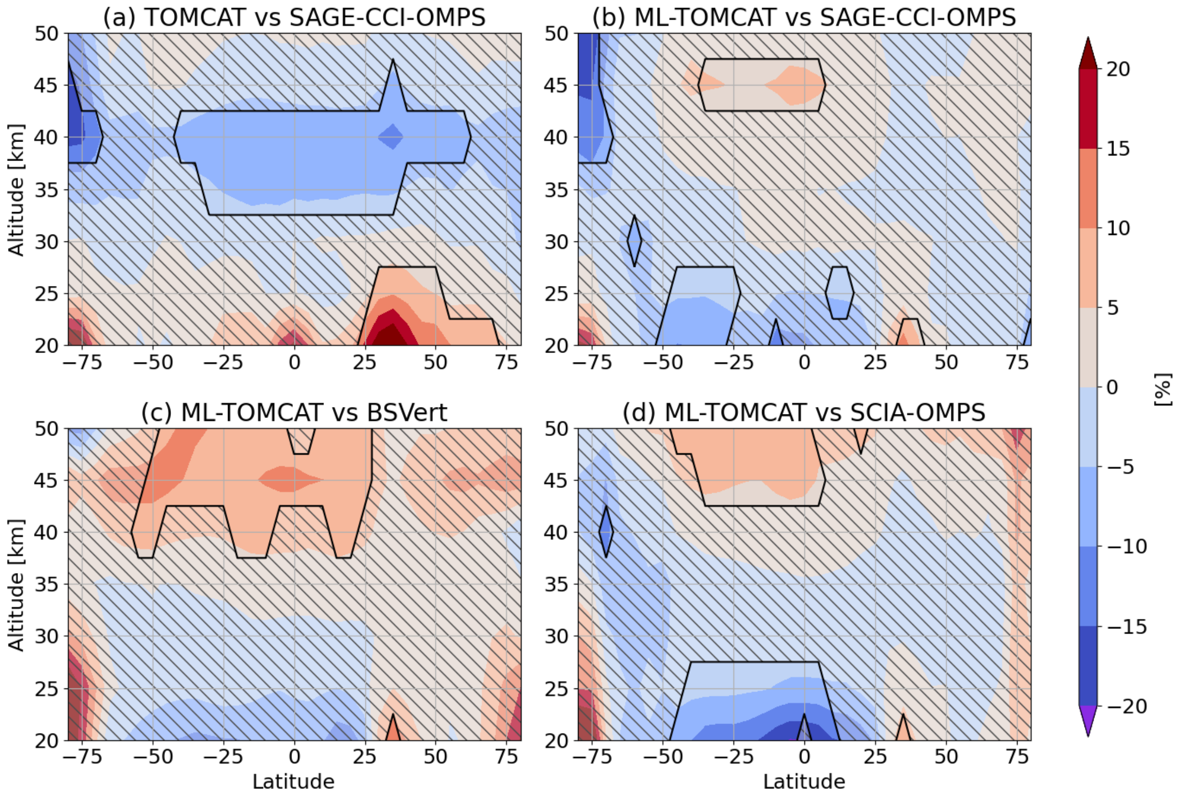

Figure 6. Relative difference (%) as a function of latitude and altitude between (a) TOMCAT ~~, ML-TOMCAT~~ versus SAGE-CCI-OMPS (1985-2019) and ~~the three considered datasets:~~ ML-TOMCAT versus (b) SAGE-CCI-OMPS (1985-2019), (c) BSVert (1985-2017) and (d) SCIA-OMPS (2002-2019), averaged over the respective time series. Stippling indicates regions where differences are statistically insignificant.

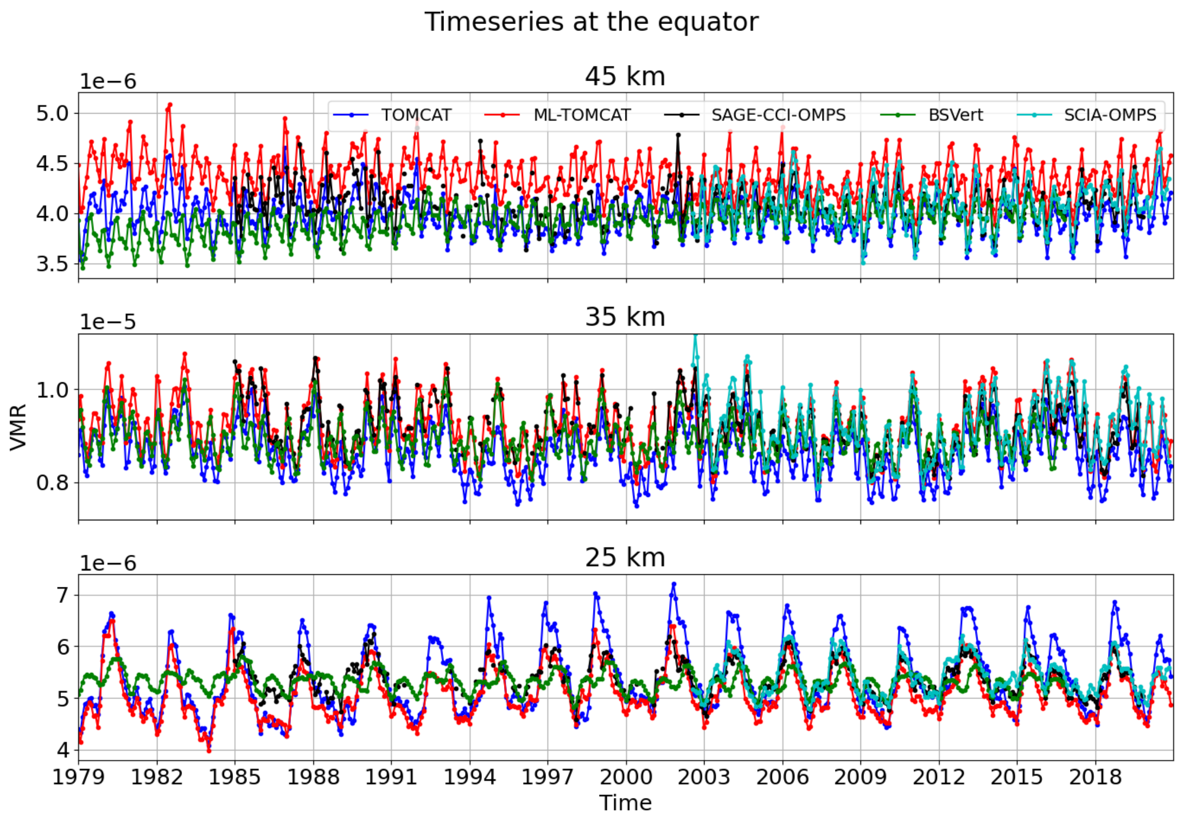

Figure 7. Comparison between TOMCAT (blue lines) and ML-TOMCAT (red lines) ozone mixing ratios over the equator (0°) at (a, top) 45 km, (b, middle) 35 km and (c, bottom) 25 km. Satellite-based ozone mixing ratios from SAGE–CCI–OMPS, BSVert (Hassler et al., 2018a) and SCIA-OMPS (Arosio et al., 2019) ~~datasets~~ data sets are shown with black, green and ~~cyan coloured~~ cyan-coloured lines, respectively.

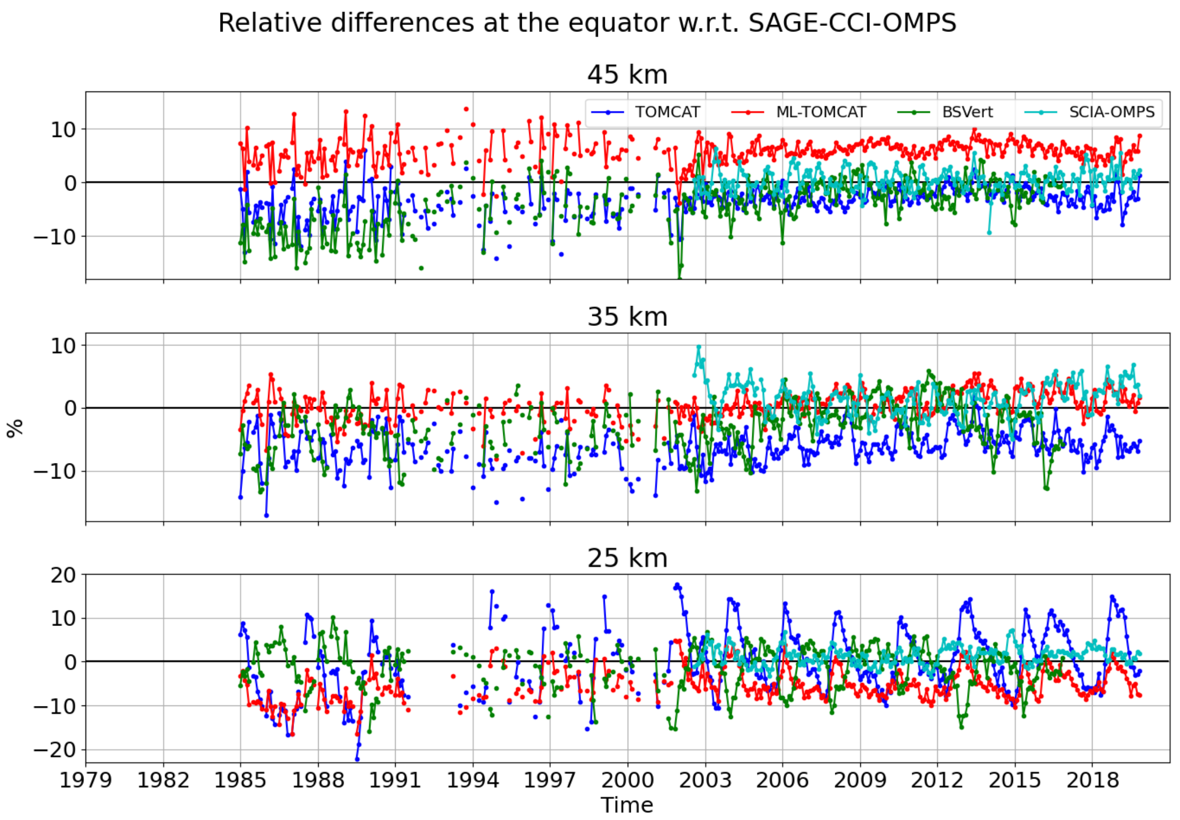

Figure 8. Same as Figure 7 but for the residuals, i.e. relative differences between TOMCAT (blue), ML-TOMCAT (red), BSVert (green) and SCIA-OMPS (cyan) ozone with respect to SAGE–CCI–OMPS.

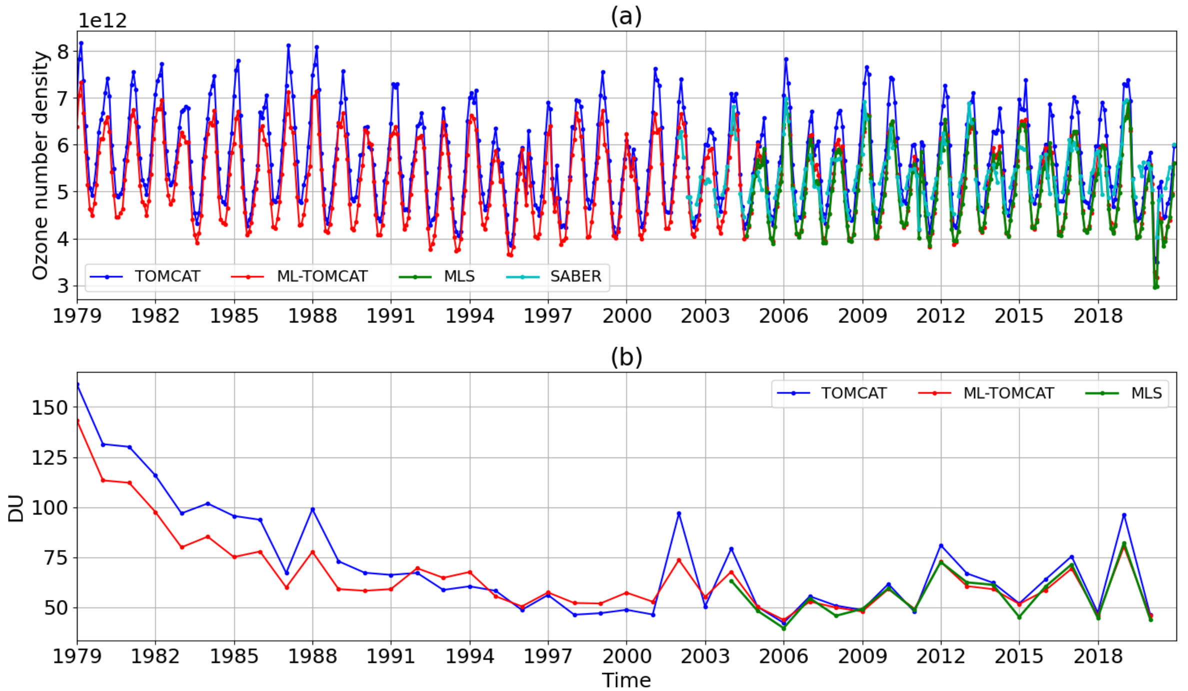

Figure 9. (a) Ozone concentration time series (molecules cm^{-3}) at 18 km over the ~~North Polar~~ Arctic region (latitudes poleward of 70°N). Aura-MLS and the Sounding of the Atmosphere using Broadband Emission Radiometry (SABER, Rong et al., 2008) data are superimposed on TOMCAT and ML-TOMCAT ~~timeseries~~time series. (b) Mean ozone sub-column (DU) between 12-20 km for September and October each year over the ~~South Polar~~ Antarctic region (latitudes poleward of 70°S).